



## Article

# Landsat 9 Transfer to Orbit of Pre-Launch Absolute Calibration of Operational Land Imager (OLI)

Raviv Levy <sup>1,\*</sup>, Jeffrey A. Miller <sup>1</sup>, Julia A. Barsi <sup>1,2</sup>, Kurtis J. Thome <sup>2</sup> and Brian L. Markham <sup>2</sup>

<sup>1</sup> Science Systems and Applications, Inc., NASA/GSFC, Code 618, Greenbelt, MD 20771, USA; jeffrey.a.miller@nasa.gov (J.A.M.); julia.a.barsi@nasa.gov (J.A.B.)

<sup>2</sup> NASA Goddard Space Flight Center, Greenbelt, MD 20771, USA; kurtis.thome@nasa.gov (K.J.T.); brian.l.markham@nasa.gov (B.L.M.)

\* Correspondence: raviv.levy@ssaihq.com or raviv.levy@nasa.com; Tel.: +1-301-614-6728; Fax: +1-301-614-6695

**Abstract:** Landsat 9 Operational Land Imager (L9-OLI) was launched on 27 September 2021, after completing a successful radiometric pre-launch calibration and characterization phase. The radiometric math model that governs the ground system—the data processing and analysis system (DPAS)—uses various calibration parameters that had been derived based on the pre-launch tests and analysis. During the on-orbit commissioning phase, the OLI system acquired specific sets of data collects, which enabled the revalidation of the pre-launch absolute calibration scale and other associated instrument performance characteristics. The analysis results shown in this paper focus on the activities and results related to the transfer-to-orbit analysis for the SI-traceable pre-launch radiometric scale. Key topics discussed in this paper include: radiance and reflectance calibration parameters for OLI; solar diffuser collects; stimulation-lamp collects; dark response; signal-to-noise ratios; and noise characteristics; radiometric response stability and the on-orbit update to the radiance to reflectance conversion factors. It will be shown that the OLI response during the early on-orbit operation matched pre-launch results and therefore this re-validates the absolute radiometric scaling at the predicted pre-launch level within the expected level of uncertainties. The launch did not cause any significant changes to the OLI system from the perspective of the absolute radiometric calibration performance. Once the transfer to orbit of the absolute calibration was confirmed, it created a solid basis for further on-orbit refinements of the radiance calibration parameters. As such, follow-on calibration refinements are discussed in other articles within this special issue, and they address issues such as uniformity as well as cross-calibration activities.

**Keywords:** Landsat; OLI; traceability; uncertainty; solar diffuser panel; in-orbit calibration; radiometric response stability



**Citation:** Levy, R.; Miller, J.A.; Barsi, J.A.; Thome, K.J.; Markham, B.L. Landsat 9 Transfer to Orbit of Pre-Launch Absolute Calibration of Operational Land Imager (OLI). *Remote Sens.* **2024**, *16*, 1360. <https://doi.org/10.3390/rs16081360>

Academic Editor: Pablo Rodríguez-González

Received: 20 February 2024

Revised: 26 March 2024

Accepted: 27 March 2024

Published: 12 April 2024



**Copyright:** © 2024 by the authors. Licensee MDPI, Basel, Switzerland. This article is an open access article distributed under the terms and conditions of the Creative Commons Attribution (CC BY) license (<https://creativecommons.org/licenses/by/4.0/>).

## 1. Introduction

The Landsat 9 observatory is the latest satellite in the Landsat mission series. It launched on 27 September 2021. Similar to Landsat 8, Landsat 9 includes two imaging radiometer payloads: the Operational Land Imager (OLI), which is the subject of this paper, and the Thermal Infrared Sensor (TIRS), whose initial transfer to orbit activities are covered elsewhere [1]. The commissioning phase of the Landsat 9 observatory proceeded as planned through the end of January 2022 with no issues that impacted the radiometric quality of the payloads. As a result, all of the planned sets of collects dedicated towards the on-orbit characterizations of the payloads performance were obtained. NASA (National Aeronautics and Space Administration) transferred the observatory operations to the USGS (United States Geological Survey) for normal science operations following the post launch assessment review on 26 January 2022. Landsat 9 data collects from the two science instruments that started their operation on 31 October 2021, became available in the USGS archive on 10 February 2022. In this paper, the prime focus is on the period of the initial on-orbit operations and the activities that re-validated the radiance absolute scale uncertainty

of the Landsat 9 OLI. These collects occurred within the first month of operation of the OLI (Note that pre-launch the term OLI2 was used to identify Landsat 9 OLI. Landsat 9 OLI is the updated post launch designation. In this article, if no designation is provided, assume we discuss Landsat 9 OLI and not the Landsat 8 OLI.). In this article we follow the portion of the on-orbit collects used to demonstrate that the on-orbit absolute calibration and characteristics of the Landsat 9 OLI remained the same as it was defined pre-launch. Such early orbit operation radiometric scale confirmation is a typical activity in many remote sensing mission [2,3].

For OLI, the only expected on-orbit update that follows this validation activity is to the per-band conversion factors that link between the radiance and reflectance absolute radiometric scales. This is because the values derived from the on-orbit collects are based on true values of the top of atmosphere solar illumination. On the other hand, the pre-launch-based predictions involve atmospheric transmission corrections and test configuration transmission losses. The final values for these conversion factors will be reported in the results section of this article. Outputs from data collects related to the transfer-to-orbit analysis are presented in this article. The conclusion section will illustrate that launch did not negatively impact the OLI absolute radiometric calibration scales beyond the expected level of transfer to orbit uncertainties. This provided a basis for additional follow-up radiometric calibration refinement activities that took place throughout the remainder of the on-orbit commission period and will continue through the mission lifetime by utilizing not only the on-board system calibrators, but also vicarious calibration and global earth-based cross-calibration activities aimed towards making the two OLI systems from Landsat 8 and Landsat 9 work as one. Some of these follow-on calibration refinement updates are discussed elsewhere in this special issue [4–7]. The authors hope this publication will enable science users and other earth remote sensing systems developers to benefit from the information provided and enhance their understanding of the datasets they obtain from the Landsat 9 OLI USGS-EROS ground processing system. Furthermore, this article highlights a process in which the radiometric scales transfer to orbit traceability was evaluated. Both Landsat 8 and Landsat 9 OLI followed the same three-part process. The first part of this process involves a rigorous pre-launch calibration traced to a laboratory standard. The second part requires having an invariant reference source on-board the system (for as many spectral bands as possible), while using this source both pre-launch and on orbit for validating that the expected responses are within expected uncertainties. The third part is the need for supplementing with other on-board calibration sources for spectral bands that could not be used with the invariant source. For the OLI on-board calibration sub-system (Figure 1), the launch event invariant source on-board is the solar diffuser reflectance panel and the supplemental source is the stimulation lamp source. The ultimate results of the work discussed in this publication are condensed into the last figure of Section 3 that illustrates the transfer-to-orbit results show no need for updates of the radiance calibration scale.

### 1.1. OLI Design Overview

The Landsat 9 OLI subsystems are identical to the design of the Landsat 8 OLI system. They both utilize the same multispectral focal plane modules design of nine spectral bands covering both VNIR and SWIR [8]. For convenience, Table 1 lists relevant key parameters for these spectral bands and the maximum in band calibration sphere source signal level. The OLI is an imaging radiometer that utilizes a four-element reflective telescope and 14 focal plane modules which form the focal plane assembly (FPA). The FPA is protected from contamination with a focal plane enclosure, named the cover, and a window assembly that has an antireflection coated transmission window. For maintaining calibration on orbit, the OLI uses an on-board calibration subsystem that involves a shutter wheel, stimulation lamp assemblies that are mounted close to the aperture stop, and a solar diffuser wheel that holds a pair of space grade Spectralon<sup>®</sup> (Labsphere, Inc. North Sutton NH 03260 USA) diffusers [9–11]. The stimulation lamp assemblies (Stim Lamp or SL) have three sets

of bulb pairs that correspond to three stim lamp operational modes, named working SL, backup SL, and pristine SL, based on the frequency of on-orbit usage planned for each set. The usage plan assures both the longevity of the stim lamp subsystem and enables the tracking of the primary Working SL bulb pairs' on-orbit aging performance. As illustrated in Figure 2, each of these sets will produce a different illumination distribution on the OLI FPA after passing through the entire telescope system. The cause for the various illumination distributions is related to filament sag and the position of the bulb relative to the stim lamp transmission diffuser. This behavior of the stim lamp illustrates one of the reasons its response on orbit is not expected to repeat the pre-launch results. During the initial mission on-orbit commissioning, there had been up to 133 various special calibration-related collect sequences that utilized the on-board calibration system. In the context of this publication, we are mainly concerned with the subset of collects that utilized the working solar diffuser and the working stim lamp, as well as the reference dark collects taken with the shutter wheel. The shutter-wheel collects provide information on the dark background response and the dark noise level.

**Table 1.** OLI bands key parameters including center wavelength and associated signal levels definitions for typical (Ltyp), high (Lhigh), and saturation radiance (Lmax), along with the in-band DSS maximum calibration level radiance (L20). More details about the spectral response at <https://landsat.gsfc.nasa.gov/satellites/landsat-9/landsat-9-instruments/oli-2-design/oli-2-relative-spectral-response/> (accessed 20 January 2024).

Band Name	Center Wavelength [nm]	Radiance Levels Definitions [W/m <sup>2</sup> sr μm]			
		Ltyp	Lhigh	Saturation Spec Lmax	Sphere Source Max Calibration Level L20
Coastal Aerosol	443	40	190	555	598
Blue	482	40	190	581	671
Green	562	30	194	544	629
Red	655	22	150	462	550
NIR	865	14	150	281	309
SWIR 1	1610	4	32	71.3	69.7
SWIR 2	2200	1.7	11	24.3	22.9
Pan	590	23	156	515	606
Cirrus	1375	6	N/A	88.5	90.7

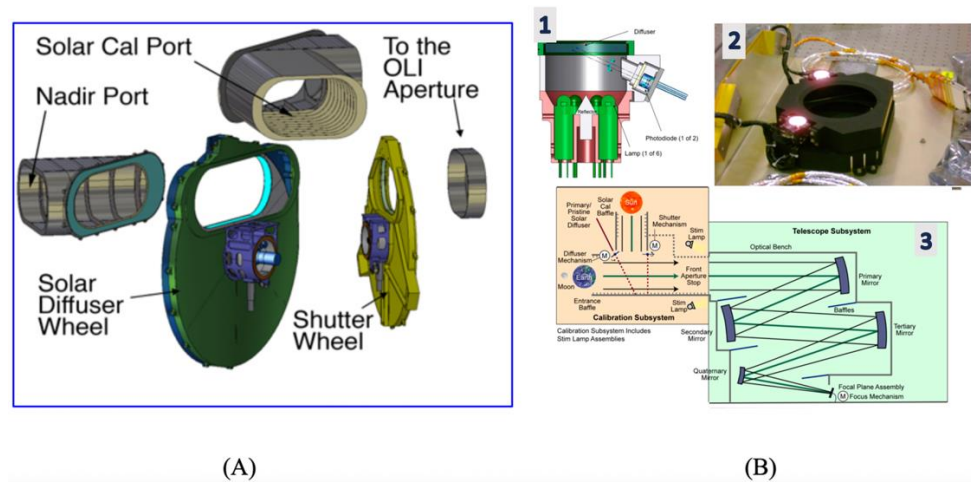


**Figure 1.** (A) OLI-1 and OLI-2 calibration assembly diagrams. ((B)-1) OLI stimulation lamp assembly drawing; ((B)-2) OLI lamp assemblies mounted on OLI aperture stop; and ((B)-3) calibration device locations in OLI optical path. Diagrams and photograph are courtesy of Ball Aerospace & Technologies Corp., 1600 Commerce Street, Boulder, CO 80301, USA [10].

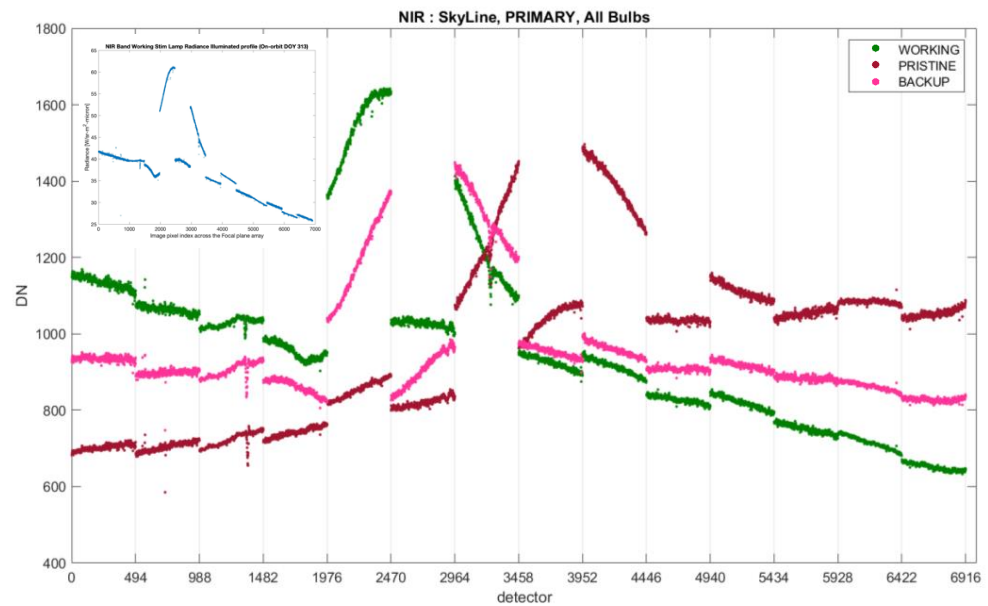


**Figure 2.** Samples of FPA response plots showing the distinctive patterns for the net signal of each of the three configurations of lamp pairs when operating with the primary electronic side of the OLI (as operated on orbit). The inserted box plot is the calibrated radiance plot for the working lamp pair, which illustrates the non-uniform radiance profile (as measured on 2021 DOY 313). The two-dimensional non-uniform illumination on the focal plane sampled by the staggered 14 modules, even after full radiometric processing, cause what appear to be discontinuities in the OLI response. These discontinuities are only an artifact of the illumination non-uniformity. It illustrates one of the causes for expecting higher uncertainties when evaluating the transfer to orbit with the SL calibration device compared to the solar diffuser panel device.

### 1.2. Pre-Launch Absolute Radiometric Scale and Related Uncertainties Overview

During the integration and tests of the OLI system and its subcomponents we have collected the FPA response datasets that track the stim lamp response, dark response, and solar diffuser response. The OLI solar diffuser response was evaluated in a unique collect configuration that provided a bottom of atmosphere (BOA) solar illumination delivered into the OLI system while it was inside the thermal-vacuum chamber. This acquisition configuration using a heliostat illuminated the actual absolute reflectance reference panels (the flight solar diffuser panels). This set of heliostat collects is part of the pre-launch steps involved with transferring the National Institute of Standards and Technology (NIST) traceable calibration collects made at the University of Arizona remote sensing lab onto the OLI FPA response [12]. Daily stim lamp radiometric collects occurred in temporal proximity to the primary radiometric calibration collects viewing a large integrating sphere source (also known as the “DeathStar” Source (DSS)). The integrating sphere collects with the DSS are the primary path for the NIST traceable absolute radiance scale of the OLI system. The readers should note that both Landsat 9 and Landsat 8 OLI utilized the same tools and methods to establish the radiometric scaling. A few improvements were made to the implementation methods used in the Landsat 9 collects. These aimed to enhance the uniformity and the non-linearity characterization. For Landsat 9 OLI the pre-launch calibration benefited from a fresh new re-characterization of the diffuser transfer panels at NIST ROSI [13] and the small transfer sphere source at the NIST FASCAL [14,15] facility. In addition, all transfer radiometers and analytical spectral devices (ASD) used by calibration teams and affiliates for activities related to Landsat 9 calibration had participated in a round robin campaign at Goddard Space Flight Center radiometry lab.

Applying lessons learned from the Landsat 8 pre-launch calibration, the Landsat 9 OLI involved 20 DSS signal levels that spanned the desired dynamic range and were controlled in-band for each of the OLI spectral bands. Additional non-linearity characterization

datasets were collected utilizing the focal plane integration time sweep (ITS) [16]. This set of non-linearity characterization collects occurred while viewing the stim lamp, as well as during a subset of the DSS collects covering a minimum of three DSS signal levels. These collects assisted in producing the reciprocity datasets that assisted in refining the non-linearity characterization of the OLI detectors across a wide dynamic range. Figure 3 illustrates that in the worst case of the CA band the non-linearity characterizations cover both the expected on-orbit top of atmosphere solar diffuser signal as well as the stim lamp signal with a minimum of one data point for each of the signal zones. Other important radiometric scale-related collects that occurred pre-launch involved datasets that defined the OLI full-system relative spectral response data [17,18] and sequences that evaluated the OLI system noise as well as response stability and repeatability over various time intervals. All of these collects and follow-on analysis established the per-band pre-launch radiometric scales' total uncertainties as shown in Tables 2 and 3. As both tables demonstrate, the total radiometric scale uncertainties for the DSS source-based calibration and the reflectance scale calibration are below (by a fair margin) the expected Landsat radiance and reflectance absolute accuracy level reported for science users ( $\pm 5\%$  and  $\pm 3\%$   $k = 1$  respectively [19]). As shown in the tables, the total uncertainty values are derived from the combined RSS from multiple terms from the calibration process as well as the initial reference source known value uncertainties, which are traced to NIST reports via additional laboratory collects that defined the radiometric scales pre-launch with their relevant traceability associated uncertainties. In both Tables 2 and 3 the SWIR bands, in general, and the SWIR2 and Cirrus bands, in particular, hold higher uncertainties. As it has been reported in other laboratory calibration tests [20], key factors impacting these bands' uncertainty include the baseline NIST-provided uncertainty, the ambient atmospheric transmission impact, and the stability of the calibration sphere source control loop. Such factors lead to a comparably worse response repeatability when transferring the DSS scale of the SWIR2 and Cirrus bands onto the OLI. Furthermore, unlike other OLI spectral bands that use a small sphere source as the basis for the radiance scale transfer, the Cirrus band DSS radiance NIST scale transfer path starts with an FEL lamp source. The bolded total uncertainty values listed in Tables 2 and 3 are an important reference for the transfer-to-orbit analysis approach that will be described in Section 2.

**Table 2.** OLI pre-launch radiance uncertainty ( $k = 1$ ) performance for signals of 0.3 L<sub>typ</sub> to 0.9 L<sub>max</sub>.

Uncertainty Contributing Factors	Uncertainty Level [%]								
	Coastal Aerosol	Blue	Green	Red	NIR	SWIR 1	SWIR 2	Pan	Cirrus
Reference Sphere Source Radiance Unc.	1.76	1.56	1.46	1.43	1.42	1.61	1.82	1.68	2.37
FFOV non-uniformity of calibration source	0.19	0.22	0.32	0.29	0.27	0.30	0.51	0.24	0.23
OLI Long-Term Stability	0.40	0.20	0.20	0.10	0.10	0.20	0.10	0.10	0.10
<b>Total Radiance Uncertainty</b>	<b>1.81</b>	<b>1.60</b>	<b>1.51</b>	<b>1.46</b>	<b>1.45</b>	<b>1.65</b>	<b>1.89</b>	<b>1.70</b>	<b>2.38</b>

**Table 3.** OLI pre-launch reflectance uncertainty ( $k = 1$ ) performance for signals of 0.3 L<sub>typ</sub> to 0.9 L<sub>ax</sub>.

Uncertainty Contributing Factors	Uncertainty Level [%]								
	Coastal Aerosol	Blue	Green	Red	NIR	SWIR 1	SWIR 2	Pan	Cirrus
Diffuser-measured BRDF	1.40	1.30	1.10	1.00	1.00	1.40	1.70	1.40	1.70
Geometric Uncertainty	0.87	0.87	0.87	0.87	0.87	0.87	0.87	0.87	0.87
Stray light	1.00	1.00	1.00	1.00	1.00	1.00	1.00	1.00	1.00
OLI residual non-linearity	0.50	0.50	0.50	0.50	0.50	0.50	0.50	0.50	0.50
FFOV non-uniformity (Reflectance Panel)	0.19	0.22	0.32	0.29	0.27	0.30	0.51	0.24	0.23
Long term stability	0.40	0.20	0.20	0.10	0.10	0.20	0.10	0.10	0.10
<b>Total Reflectance Uncertainty</b>	<b>2.04</b>	<b>1.95</b>	<b>1.83</b>	<b>1.76</b>	<b>1.76</b>	<b>2.03</b>	<b>2.27</b>	<b>2.01</b>	<b>2.23</b>

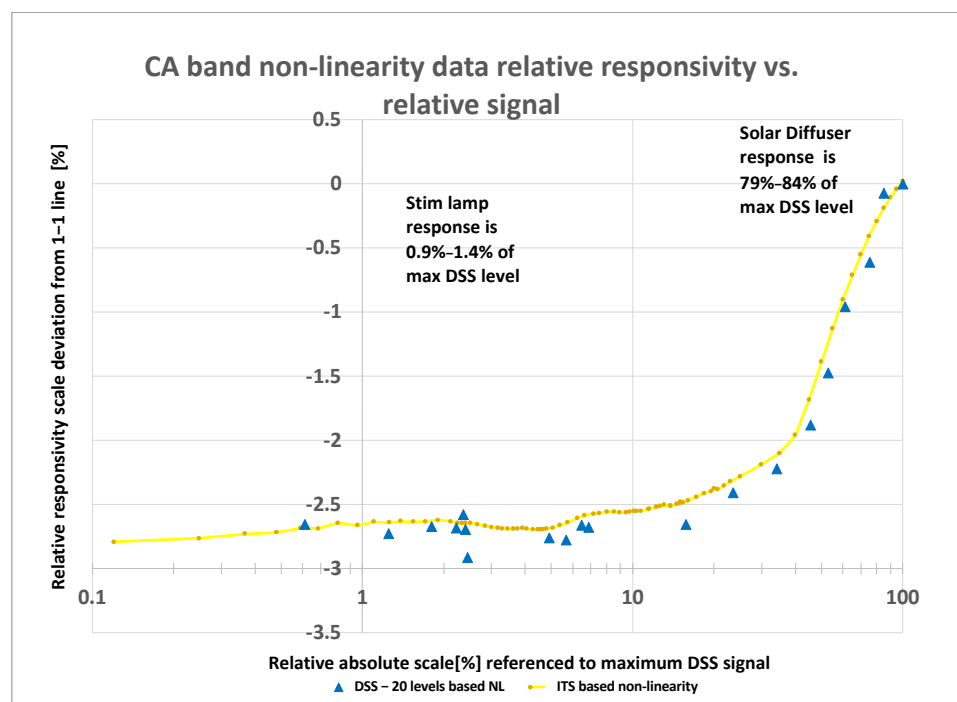


**Figure 3.** Plot of the non-linearity response characteristics shown here as relative responsivity vs. relative signal for the coastal aerosol band. The plot illustrates that the non-linearity information covers the range of expected on-orbit solar and lamp signal levels (shaded blue zones) and that the residual non-linearity error will be  $<0.5\%$  (looking at the scatter of the DSS points after the ITS-based correction is applied) at these signal levels and throughout the dynamic range of the OLI response. The plot includes both the final non-linearity correction reference as defined by the integration time sweep datasets shown in the yellow line with orange dots and the direct 20 DSS levels shown by the blue triangles. The CA band is considered the worst case scenario because the signal gap between the solar diffuser and the SL are different by nearly two orders of magnitude.

### 1.3. On-Orbit Activities Planned for Absolute Radiometric Scale Revalidation

As mentioned above, only a limited set of collects are involved with reaffirming the absolute calibration on orbit and these are mainly utilizing the following three on-board calibration test objects: the shutter, the working solar diffuser panel and the stim lamp. These collect activities are configured in one of two possible collect modes. One collect mode is with nominal integration time and the other is with the integration time sweep collects that provide a set of 21 repeated collects for each test object at variable integration time (more details about the integration time sweep collect are in [16]). All collects produce files with 500 frames for each test object. For the stim lamp collects there is a warmup duration of 185 s prior to recording the 500 frames of the collect. Waiting for the lamp warmup period assures the most repeatable slow-drifting response has been reached. One of the key assumptions in the transfer-to-orbit calibration is that reflectance properties for the solar diffuser panels are invariant throughout the launch. Therefore, changes in the radiance response on orbit are expected to be within the pre-launch defined uncertainties of the predicted values derived from the heliostat collects and analysis. If the on-orbit results are within two-sigma of the expected uncertainties, it is considered a successful revalidation of the radiometric scale. This means there is no significant shift to instrument band level mean radiance response calibration. For the Cirrus bands there was no valid heliostat data because of the extreme BOA signal attenuation. Therefore, for the Cirrus spectral band, the transfer-to-orbit evaluation was done with the SL calibration source, which operates in vacuum conditions both during the pre-launch and on-orbit collects. Once the radiance absolute scale was confirmed with the solar diffuser datasets, we addressed the remaining Cirrus band absolute scale confirmation via the use of the stim lamp data on orbit. We

expected that any radiance changes to the stim lamp response were due to variation in the on-board stim lamp signal and not due to the OLI response. The main reasoning for the stim lamp radiance expected measurable change was the “color temperature” shift, i.e., change to the spectral output. We quantified the impact of this expected spectral shift during on-orbit operation using most bands, excluding the Cirrus band and the Pan-chromatic band, by comparing the results to the pre-launch results. Lastly, we evaluated the residual error for all bands, and particularly the Cirrus band, after accounting for the spectral shift correction. To assure the overall radiometric scales were matching the pre-launch values we repeated the analysis on multiple on-orbit datasets to evaluate the illuminated response and background repeatability and stability over the commissioning period.

## 2. Method Description

The on-orbit revalidation of the Landsat 9 OLI radiometric scale involved mimicking and building on the approach used during the Landsat 8 OLI on-orbit absolute scale revalidation [10]. For that reason, the details discussed in this segment mainly cover an overview of the methodology and the modifications or additions made in the Landsat 9 transfer-to-orbit radiometric scales revalidation as deeper technical details of specific collects can be found in the provided Landsat 8 references. Expanding on the process description mentioned in Section 1 we describe what is involved in each of the three parts. In the first part, we conducted the rigorous pre-launch calibration traced to a laboratory standard, along with radiance data collects for the sun-illuminated flight solar diffuser reflective panel. This panel reflectance was expected to remain stable through the launch event. Well-defined uncertainties were derived for all pre-launch measurements. In the context of this article, we only show the final results associated with this portion. The second part involves early on-orbit repeat observations that revalidate that the responses are within the expected uncertainties for the radiance response from the sun-illuminated solar diffuser panel. A reaffirmation of the assumptions about panel reflectance scale invariance was achieved by comparing between the pre-launch and on-orbit radiance errors relative to the response expected for several Exo-Atm solar irradiance models. These will be the core of the discussion for this article, as we focus on the early on-orbit data. The third and last part resolves the missing information for spectral bands that could not be validated with the solar diffuser panel because the pre-launch data did not exist or was not valid. In that case, which mainly involved the Cirrus spectral band, we supplemented the data with a secondary on-board cal source. This source had both pre-launch and on-orbit data stable enough in any operational configuration to evaluate the transfer-to-orbit impact after adjustments for the source-related transfer-to-orbit changes were addressed. For OLI, this secondary source was the stim lamp source. As the focus of this article is on the on-orbit data, we mainly discuss and show results for the second and third part of the transfer-to-orbit process.

For Landsat 9 OLI, the pre-launch calibration results and analysis were used as a baseline for the radiance and reflectance absolute scales along with their associated calibration parameters. As illustrated in Tables 2 and 3, the pre-launch uncertainties related to those absolute radiometric scales, when considering the transfer to on-orbit operation, were mainly impacted by the instrument-measured noise levels, estimated long-term stability during on-orbit operation, and the residual error for the non-linearity correction over the full dynamic range of the system. On-orbit data was used to revalidate this portion of the uncertainty roll-up contribution by repeating the same pre-launch data collects and demonstrating that the on-orbit band-level performance for the noise, long-term stability, and the residual error for the non-linearity correction were at the same levels seen pre-launch. To complete the on-orbit revalidation of the radiance scale, we show that our measurement on-orbit results were within the two-sigma range of uncertainty that was anticipated by the pre-launch tests. As mentioned earlier, an additional underlying assumption made was that the absolute reflectance scale would remain invariant through launch, because the reference reflectance solar diffuser panels that define that scale are part of the on-board

calibration system. In that case, assuming that no change to the panel reflectance and BRDF characteristics occurred, the reflectance scale was transferred directly to on-orbit operation without any additional errors or adjustments. It is important to note that included among the several contributing factors in the pre-launch reflectance uncertainty totals are budgeted geometry-related factors that allow some level of mounting and angular changes between the pre-launch and on-orbit operation. Since signal levels collected when viewing the solar diffuser both on orbit and pre-launch were not repeating the known DSS signal levels, the residual non-linearity correction error was added as a factor to the reflectance scale uncertainty budget.

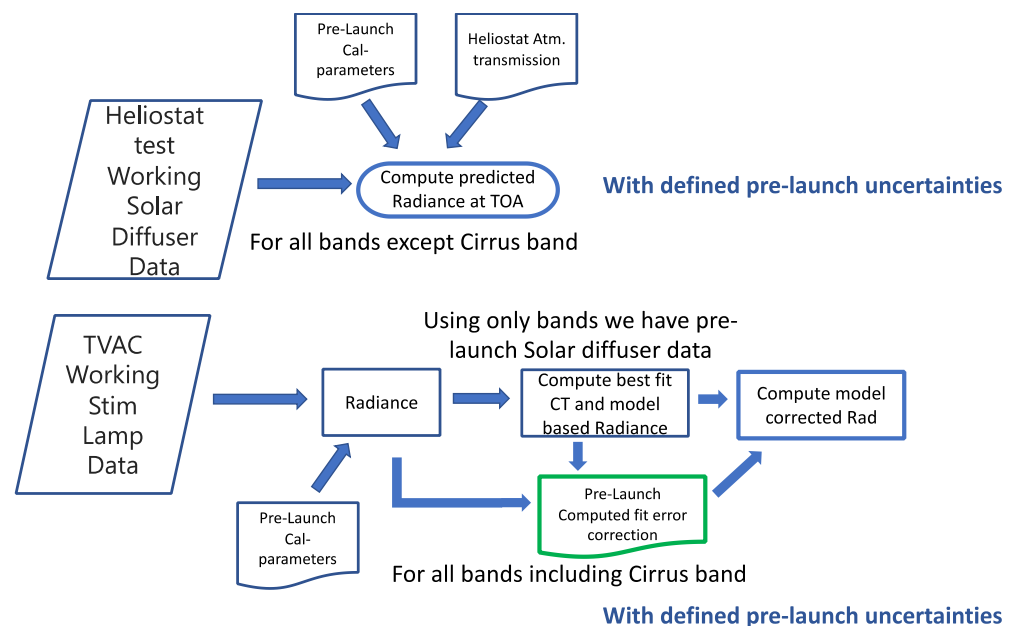
Since the OLI has two independent NIST-traceable radiometric paths, the USGS processing system uses per band calibration parameters that tie together the two absolute radiometric scales. These parameters are known as the reflectance conversion factors, and they are expected to have an on-orbit update. The initial pre-launch conversion factors were based on the predicted top of atmosphere (TOA) results derived from the heliostat data, while the on-orbit data had fewer uncertainty factors compared to the pre-launch heliostat test configuration. While this activity was not critical for the evaluation of the transfer to orbit, it involved a calibration parameter update that occurs on orbit following the revalidation of the radiance scale that is discussed in this article. On orbit, the OLI-measured TOA solar diffuser radiance values were processed following the same steps applied during the Landsat 8 OLI commissioning update of the same conversion factor parameters [10]. Differently from the core transfer-to-orbit analysis, to increase the confidence in the updated values, the final values were obtained only towards the end of the commissioning period. This assured that the values obtained included all calibration parameter refinements and all relevant datasets throughout the on-orbit commissioning period and that all were reviewed.

New for Landsat 9, the on-orbit residual non-linearity error evaluated was enhanced by utilizing integration time sweep collects made at two signal levels (solar diffuser-illuminated and SL illumination). In contrast, Landsat 8 OLI only used the solar diffuser-illuminated integration time sweep datasets. This update expanded the dynamic range of the on-orbit non-linearity performance assessment. Another update was in the analysis of the pre-launch and on-orbit SL color temperatures model fits and related residual model error estimates. While the color temperature fit process is the same, adjustment to the model by a fixed error term for all spectral bands that ties the SL results to the solar diffuser results was added. This additional term accounts for systematic changes in the SL operation on orbit that were impacted by the different operating temperature, as well as by the different transmission via the lamp's diffuser that was not captured by the color temperature model.

For evaluating the signal to noise ratio (SNR) and signal stabilities, both dark and illuminated data sources were used on orbit and processed similarly to pre-launch characterizations. Repeated SL observations, at a rate of once per day, and repeated solar collects enabled the monitoring of the stability of the response during the commissioning period. The trending analysis of these collects assisted in finding the earliest time after which the Landsat 9 OLI response stability approached a nominal steady-state. Additional special Landsat 9 OLI collects during commissioning that assisted in further re-affirming the results of the transfer to orbit (but not discussed in this paper) are the Landsat 8 and Landsat 9 cross-cal activities that involved both the underfly [6,7] as well as experimental near-simultaneous working solar diffusers and lunar collects.

Illustrated in Figure 4a,b are the overview analysis flows for the solar diffuser data and the stim lamp datasets during pre-launch and on orbit. These flow plots highlight the steps of data processing and analysis involved with the radiance transfer-to-orbit revalidation for both the second and third parts of the process. Plot 4(a) shows that the first part of the transfer to orbit involved the pre-launch heliostat test data collects, when the OLI views the working solar diffuser while illuminated with BOA solar radiance. From these collects we obtained the measured radiance using pre-launch calibration for all bands. From the BOA solar diffuser response, we computed the TOA-predicted radiance levels

after correcting for the atmospheric transmission as measured for the days of the heliostat collects and normalized to the 1[AU] earth–sun distance condition. As described by Jeffrey Czaplá-Myers, who conducted the pre-launch analysis for the heliostat test configuration, the analysis involved for these pre-launch collects utilized multi-spectral channel solar radiometers from which various atmospheric parameters, their associated uncertainties, and the scattering phase function were obtained (parameters involved were the total optical depth, the Rayleigh optical depth, the aerosol optical depth, the ozone optical depth, and the Angstrom exponent). These were then used as input into MODTRAN [21]. Ultimately, the MODTRAN radiative transfer model was used to determine the 350–2500 nm spectral range atmospheric transmission along with the overall system transmission, and the spectral bands enabled the computation of the in-band average transmission in every spectral band except for the Cirrus band. The predicted TOA radiance-associated uncertainties were dependent on the sources of uncertainty associated with the heliostat collect and involved the heliostat test total transmission, the Thuillier solar exo-atmospheric spectral irradiance model uncertainties, and the OLI radiance scale uncertainty (See Table 1 in [22]). The processing involved in the conversion of the measured OLI response into radiance used the official pre-launch calibration parameters, the measured heliostat test configuration transmission, and the atmospheric transmission. The radiance was transformed from BOA to TOA-predicted values for all bands except for the Cirrus band. In order to demonstrate high confidence in the results, in Section 3 we report the on-orbit processed solar diffuser data from two independent processing systems. While both follow the same computation base model for converting digital counts to the traceable International System of Units (SI) of radiance, each has slightly different independently derived calibration parameters and non-linearity corrections. One system was the USGS official processing system and the other was the Ball Aerospace & Technologies Corporation (BATC) system.



(a)

Figure 4. Cont.

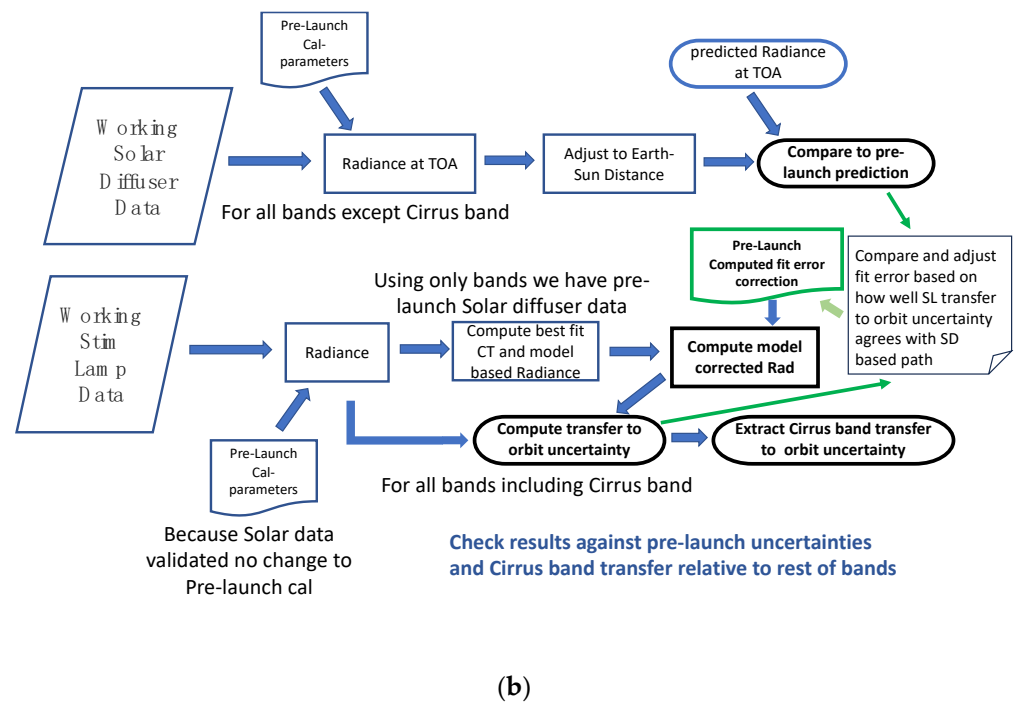


**Figure 4.** Flowchart of the transfer-to-orbit analysis steps for solar diffuser and stim lamp datasets in both pre-launch and on-orbit collect modes. (a) Pre-launch collects analysis steps for solar diffuser and stim lamp data. (b) On-orbit collects analysis steps for computing the transfer-to-orbit uncertainty for both solar diffuser -based path and stim lamp-based path. Final analysis outputs that will be shown in Section 3 are shown in (b) in bolded black frames. For stim lamp analysis, new color temperature fit results are computed. Initially, the same fit residual error correction as from pre-launch (green highlighted frame) is applied; later, it is adjusted by fixed correction bias for all bands to force agreement between the SD and SL-based analysis results (shaded note with the thick green arrow feedback to the initial model error).

During the pre-launch phase analysis, the working stim lamp spectral output characteristics were modeled as an effective color temperature blackbody source. The spectral radiance of the working lamp was computed in a three-part fit model. Part one was an effective color temperature, the second part was a scaling factor, and the last part was a residual error to the modeled fit output. The model fit was restricted to using only select spectral bands (excluding the Cirrus band and the spectrally wide panchromatic band) so that their absolute radiance scale could be revalidated directly with the diffuser datasets. All working stim lamp data were converted into radiance units using the official pre-launch calibration parameters. Then, the model fit parameters were computed along with the pre-launch relative residual-fit error between the model and actual response for all spectral bands. This included the error for the Cirrus and Pan bands to the same stim lamp model fit. Lastly, if no on-orbit changes occurred to the OLI system layout, the OLI detectors' response, and the overall optical transmission of the SL system, it was correct to use the pre-launch-derived relative residual-fit error correction between the model fit and the actual radiance. This residual relative error was assumed to be invariant throughout the launch for all spectral bands and within the expected small change to the "effective" color temperature of the SL. Any residual errors associated with this assumption would show up as an additional single value scaling correction that could be applied to all bands to make the stim lamp transfer-to-orbit match the solar diffuser transfer-to-orbit results.

On orbit, we conducted similar data collects of the working solar diffuser and the working stim lamp. The solar diffuser data were converted into radiance with the official pre-launch calibration parameters, and after adjustments to the day of the year, which impacts the earth–sun distance correction factors, it was compared to the predicted pre-

launch values for the TOA working diffuser radiance for the same date in which the heliostat collects happened. With no additional error and noise uncertainties present, the results are expected to be within the range of uncertainty predicted by the heliostat uncertainty analysis. The results of the TOA actual radiance vs. the pre-launch predicted radiance were compared. If the results demonstrated a significant change that required an update to the on-orbit calibration parameters, a preliminary adjustment would be made to the pre-launch radiance scale calibration parameters prior to the assessment of the stim lamp on-orbit response. In that case, the measurement of the working pair stim lamp would be processed into radiance with the updated on-orbit calibration parameters. For Landsat 9 OLI, since no change was needed, the official pre-launch calibration parameters were used. With this radiance data, and using the same spectral bands used during the pre-launch color temperature-model fit, a new color temperature-model fit was calculated. After applying the pre-launch-derived relative-fit error correction to the model fit in all bands we computed a new on-orbit model-derived radiance. The remaining difference in the error between the model computed radiance and the actual SL radiance for all bands is the initial estimate for the transfer-to-orbit impact. In the last step, we estimated an additional flat offset correction for making the SL-based residual error better matched to the solar diffuser-based results. This offset adjustment factor corrects the SL model, to better reflect the transfer-to-orbit effects of the OLI system alone. However, from an uncertainty point of view, this added factor carries the most significant portion of the uncertainty associated with the SL path for validating the transfer to orbit. Lastly, we report the Cirrus band SL-derived transfer-to-orbit residual error result and again compare it to the range of known uncertainty terms.

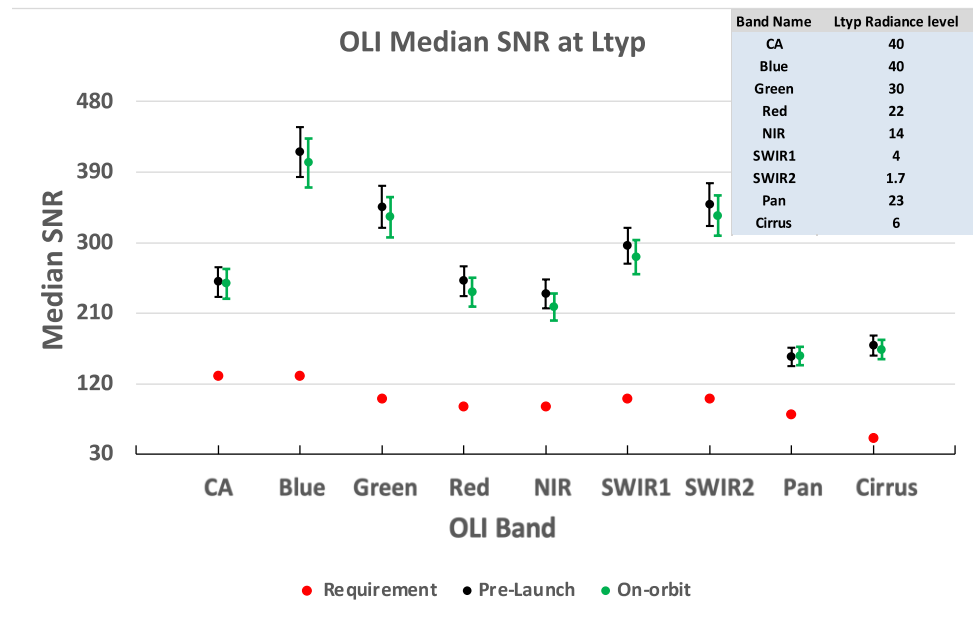
### 3. Transfer-to-Orbit Analysis Results and Discussion

This section is organized into three parts that will cover the analysis results that reaffirm the OLI absolute radiance scale. The first part covers the OLI response stability, signal-to-noise values, and residual non-linearity. The second part covers the results of the OLI working solar diffuser-based, transfer-to-orbit impact evaluation. The last part covers the OLI working stim-lamp-based, transfer-to-orbit evaluation, and while it will show results for all of the narrow bandwidth spectral bands, its main role is in defining the level of the transfer-to-orbit impact for the Cirrus band absolute radiance scale.

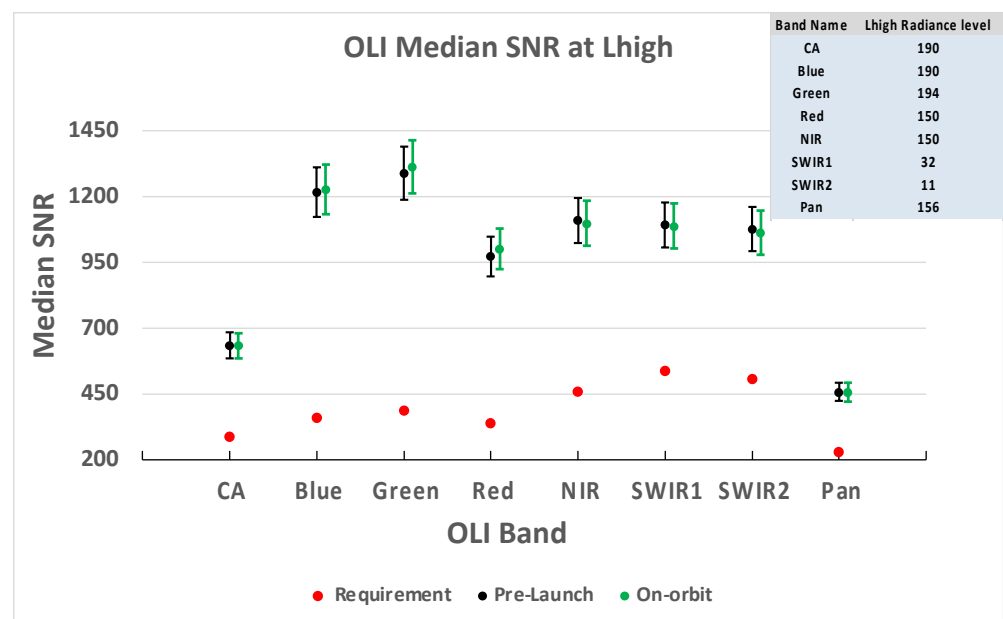
#### 3.1. OLI Response Stability, Noise Levels, and Residual Non-Linearity

The noise analysis on orbit was assessed in a similar manner to how it was assessed during the pre-launch testing, using shutter, working SL, and working solar diffuser datasets. One small difference was that, during the pre-launch, the evaluation of the SNR vs. signal relationship used the DSS-illuminated datasets and not the solar diffuser datasets. Since the OLI absolute radiance scale is a band average-level characteristic, we reported the OLI signal-to-noise, response stability, and residual non-linearity metric for the band average results. Starting with the estimated SNR, results are reported for the band median evaluated at the two signal levels of  $L_{typ}$  and  $L_{high}$  in the same manner as they were reported pre-launch. The results illustrate the worst-case conservative estimate for the SNR values shown that include a subtraction of 7.76%. The value of 7.76% is associated with the worst-case SNR-estimated uncertainty. This evaluation uses shutter dark data, stim lamp data, and either solar diffuser or DSS peak signal data to derive per-band least squares fit model parameters for the SNR vs. signal level. The total uncertainty that was associated with the SNR calculation was computed from the root sum of squares of three terms. These terms are the least square model-fit residuals, the estimated residual non-linearity, and the uncertainty in the radiometric signal. Notice that all of these terms are expected to retain their pre-launch levels, hence the uncertainty for the SNR remains a fixed value valid for both pre-launch and on orbit. From the perspective of the transfer-to-orbit analysis, it is assumed that all spectral bands and all signal levels can use the same 7.76% conservative level of uncertainty. Plotted in Figure 5a,b are the worst case median SNR at  $L_{typ}$  and SNR

at Lhigh values computed from pre-launch and on-orbit datasets with the conservative 7.76% uncertainty error bars added to both. The SNR values in Figure 5 match within the one-sigma error bar for both Ltyp and Lhigh. This confirms that no change occurred for the noise performance of the OLI on orbit. Table 4 summarizes the range in the differences for SNR between pre-launch and on orbit states for Ltyp and Lhigh for all spectral bands. This table shows that for all bands and both signal levels, the estimated SNR match is within the one-sigma level of 7.76%. The summary table shows that for Ltyp the delta ranged between  $-0.5\%$  for the Panchromatic band and  $7.1\%$  for the NIR band with a median change of  $3.8\%$  for all of the spectral bands. For Lhigh SNR, the change was between  $-2.9\%$  for the Red band and  $1.2\%$  for the SWIR2 band with a median change of  $0.3\%$ .



(a)



(b)

**Figure 5.** Pre-launch and on-orbit results for OLI worst case median SNR values evaluated at two signal levels: (a) Ltyp signal level results and (b) Lhigh signal level results. The Cirrus band does not have a defined requirement for a reference signal level at Lhigh hence it is not shown in the plot.

**Table 4.** Summary of per band SNR relative change between pre-launch and on-orbit results.

Band Name	Change in On-Orbit SNR Evaluated for Two Signal Levels	
	Ltyp [%]	Lhigh [%]
<b>Coastal Aerosol</b>	0.9	0.4
<b>Blue</b>	3.4	−0.8
<b>Green</b>	3.8	−1.9
<b>Red</b>	5.7	−2.9
<b>NIR</b>	7.1	1.0
<b>SWIR 1</b>	4.8	0.3
<b>SWIR 2</b>	4.0	1.2
<b>Pan</b>	−0.5	0.2
<b>Cirrus</b>	3.2	

The long-term stability characteristics of the OLI were defined for the response stability over the duration of the 5-year lifetime of the OLI system. The pre-launch values reported are conservative estimates of the mean with the addition of two times the standard deviation level of the OLI instability for each spectral band. The stability assessment also included an additional offset bias to account for the 5-year pristine solar diffuser panel aging degradation. The pre-launch result started with the estimated results for the 16-day short-term stability, to which is added the mean plus twice the standard deviation computed terms and an additional value of 0.028% to account for the 5-year aging degradation of the solar diffuser response uncertainty. The diffuser aging degradation impact was derived from pre-launch measurements on diffuser material witness samples that concluded that the UV exposure of the diffuser panels will cause a change of no more than 0.1% per hour of sunlight. Since the pristine diffuser total on-orbit operation over 5 years will not exceed 17 min of sun exposure, the aging impact for this duration was computed to be 0.028%.

On orbit, the estimate of the long-term stability was derived from the trending analysis of daily working SL collects and the repeated working solar diffuser collects, from which we compute the 16-day stability value and the two-sigma drift fit uncertainty. The 16-day stability drift is derived from the initial trend of nearly 70 days of OLI operation after the instrument response appeared to approach a steady state plateau (omitting the first two datasets for the SL and solar diffuser collects). To illustrate this, a plot for the on-orbit Coastal Aerosol band trending data is shown in Figure 6. The trend analysis is repeated for every band and both the solar diffuser and stim lamps datasets. The 16-day stability on-orbit results are shown in Table 5 for both the stim lamp and solar diffuser. The last line of Table 5 shows the roll-up results for the on-orbit long-term stability values that use a root sum square of three bolded-value lines to compute the total on-orbit long-term stability. The 16-day stability mean and two-sigma variation estimates from the observations of the solar diffuser panel and the SL are condensed into the two bolded-value lines. These bolded lines use the largest derived mean level for 16-day stability, from the solar diffuser and the stim-lamp datasets, in each spectral band and the smallest two-sigma stability estimate of variation in the results, from the same datasets. The rationale for using the smallest value among the solar diffuser and the stim lamp two-sigma uncertainty was due to the observation, that for both pre-launch and on orbit states, the two-sigma scatter and variability about the stability estimates were the dominating factors impacting the 5-year stability values.

Observations made during the analysis show that variation between the sources used in the evaluation between the pre-launch and on orbit states impact the resultant two-sigma levels. The on-orbit source and collect conditions repeatability are harder to control and for that reason we obtained a more correct estimate for the core OLI detector response stability when we used the smallest two-sigma values. It is interesting to note that, in general, for all spectral bands except for the CA and Blue bands, the stim lamp-based two-sigma estimate was always lower than the solar diffuser results. The last line in Table 5 shows that seven out of nine bands resulted in equal, or even lower, values compared with the pre-launch

long-term stability results. Only for the Red and Panchromatic spectral bands was the on-orbit stability estimate doubled from 0.1% to 0.2%, and their estimated two-sigma variations were as high as five times worse than the pre-launch levels. Furthermore, in the context of the transfer to orbit, these two spectral bands' change impact was less the 0.1% and it was not a significant value, especially when the results for all bands showed on-orbit-derived long-term stability values that were better than 0.2%. These results illustrated that the long-term stability on orbit during the initial 70 days of operation was at the same level predicted pre-launch. The Red and Pan spectral bands that exhibited the higher uncertainty on orbit were most likely a limitation dominated by stim lamp source stability for these spectral bands. Since during the initial 70 days of operation the spacecraft activities involved many non-routine operations, these might have induced additional instability in the SL source collects. When re-evaluating this analysis after a year of operation we found the CA 16-day stability mean value from the stim lamp data to be <0.01% rather than the 0.02%; however, the two-sigma uncertainty level was still high, most likely due to the low signal level produced by the stim lamp.

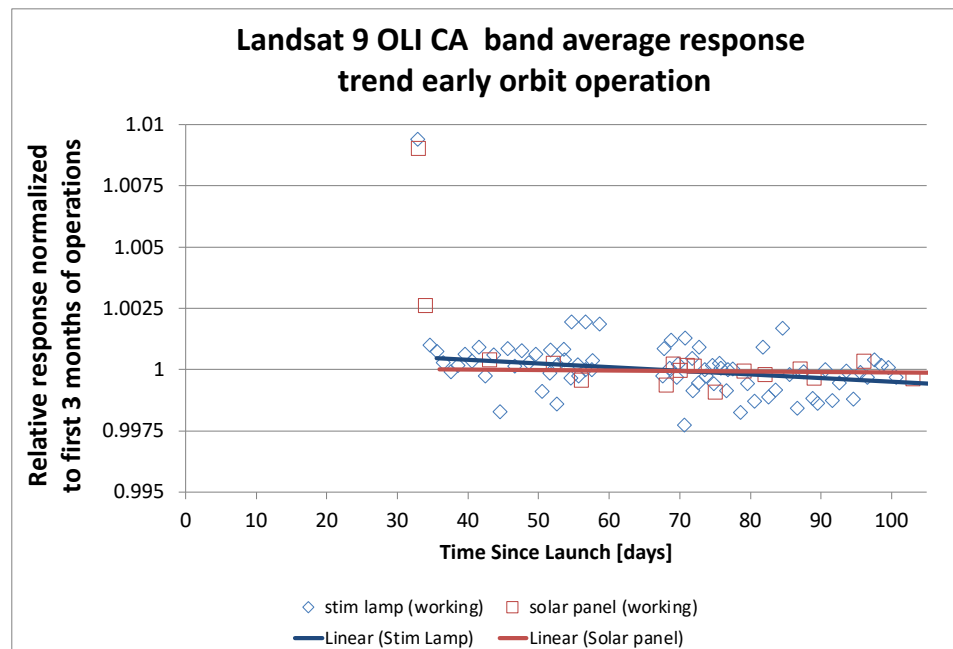


**Figure 6.** On-orbit normalized response trends for OLI CA band during the early operation from both working solar diffuser and working stim lamp datasets. This illustrates how the 16-day stability values are derived from the linear trend slopes once a steady-state response had been reached (2 days after initial turn-on).

**Table 5.** Summary of on-orbit 16-day stability parameters extracted from solar panel and SL during early orbit operation.

On-Orbit Long-Term Stability Evaluation Components	Associated Uncertainty Level [%]								
	Coastal Aerosol	Blue	Green	Red	NIR	SWIR 1	SWIR 2	Pan	Cirrus
16-day Stim lamp-based mean	0.02	0.03	0.04	0.04	0.03	0.00	0.00	0.04	0.00
16-day Solar diffuser panel-based mean	0.00	0.04	0.04	0.04	0.04	0.04	0.04	0.05	0.04
16-day on-orbit estimate	<b>0.02</b>	<b>0.04</b>	<b>0.04</b>	<b>0.04</b>	<b>0.04</b>	<b>0.04</b>	<b>0.04</b>	<b>0.05</b>	<b>0.04</b>
16-day Stim lamp-based 2-sigma variation	0.17	0.14	0.11	0.10	0.07	0.01	0.01	0.11	0.01
16-day Solar diffuser panel 2-sigma variation	0.07	0.12	0.11	0.10	0.09	0.10	0.10	0.12	0.09
16-day on-orbit 2-sigma variation estimate	<b>0.07</b>	<b>0.12</b>	<b>0.11</b>	<b>0.10</b>	<b>0.07</b>	<b>0.01</b>	<b>0.01</b>	<b>0.11</b>	<b>0.01</b>
End-of-life degradation impact	<b>0.028</b>	<b>0.028</b>	<b>0.028</b>	<b>0.028</b>	<b>0.028</b>	<b>0.028</b>	<b>0.028</b>	<b>0.028</b>	<b>0.028</b>
<b>Total long-term on-orbit stability</b>	<b>0.1</b>	<b>0.2</b>	<b>0.2</b>	<b>0.2</b>	<b>0.1</b>	<b>0.1</b>	<b>0.1</b>	<b>0.2</b>	<b>0.1</b>

The last radiometric-related performance characteristics of OLI response that we could confirm on orbit were the non-linearity characteristics. For Landsat 9 OLI, the pre-launch characterization was conducted with an improved protocol in which the signal levels were controlled in-band, and the test collect sequences enabled decoupling non-linearity from non-uniformity [11]. This improved non-linearity characterization, and enabled better understanding of the integration time sweep datasets and how they relate to radiance-based non-linearity collects. This enabled the Landsat 9 OLI to use datasets at two signal levels for the on-orbit non-linearity characterization. The addition for Landsat 9, was in the set of stim lamp integration time sweep (ITS) collects, whereas for Landsat 8 we only had the solar diffuser set of ITS collects. The updated sequence of operation produced the same 21 integration times for both the solar diffuser data and the post-warmup-period stim lamp illumination. These enabled us to track changes for the non-linearity over time, relative to the pre-launch non-linearity correction, all while covering a wider portion of the OLI's dynamic range. The analysis of these on-orbit results from this new set of integration time collects confirmed that we were correcting the non-linearity to within  $<0.5\%$  across the dynamic range for all bands [23].

Illustrated by Figure 7 is the on-orbit residual band average error after a non-linearity correction-derived pre-launch was applied. The estimated on-orbit non-linear relative error was computed in reference to the expected linear signal. The expected linear signal was computed as the product of the SL nominal signal response and the ratio of each integration time value to the nominal integration time. The horizontal dashed red line in Figure 7 illustrates the  $0.5\%$  residual non-linearity desired limit. Clearly all bands were meeting this requirement limit over two orders of magnitude in the dynamic range. Notice that, for each band, the on-orbit-derived validation started at a different maximum signal level as it was dependent on the signal viewed with the solar diffuser. Only the shorter wavelength bands of CA, Blue, and Green showed that the mean response for the ITS lamp data could jump above the  $0.5\%$  and this occurred only at signals that were below  $0.2\%$  of the dynamic range. As a reference, this signal level is about 10 times smaller than the  $0.3$  Ltyp signal (the lowest signal where OLI requirements are defined). The remaining spectral bands maintained the residual of  $<0.5\%$  non-linearity across three orders of magnitude in the dynamic range. The uncertainty associated with the residual non-linearity plot will naturally increase as the signal level decreases. The on-orbit residual non-linearity check allowed us to state with certainty that for post linearity corrections (the residual error between the peak solar diffuser and the peak stim lamp responses) the error was nearly at the level of the total long-term stability response values shown in Table 5.

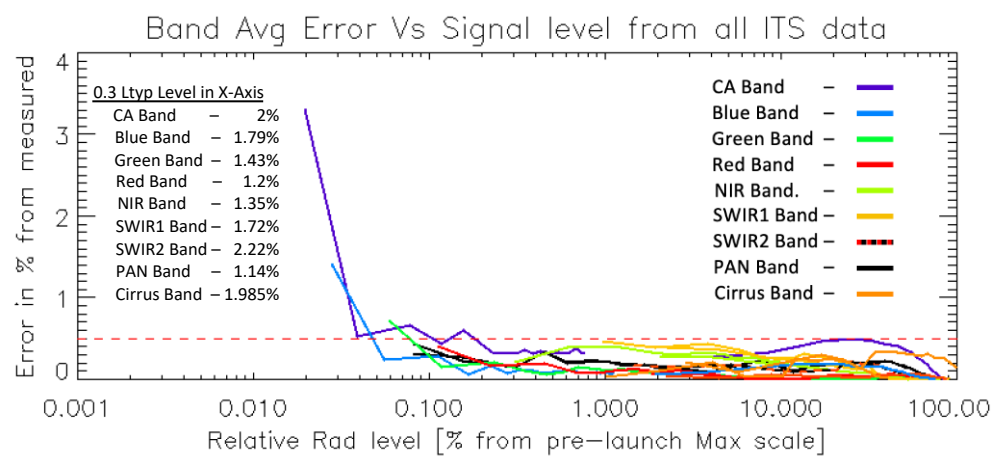


**Figure 7.** On-orbit-derived residual relative non-linearity band mean level error vs. relative signal level across the dynamic range of OLI response for all spectral bands with the  $0.5\%$  threshold shown as the horizontal dashed red line (utilizing integration time sweep data from both solar diffuser and stim lamp collects).

### 3.2. Solar Diffuser Collects-Based Transfer to Orbit

This segment focuses on the measurements of the OLI response to the on-board reflectance scale absolute calibration reference, i.e., the working solar diffuser panel, when it was sun-illuminated, both pre-launch and on orbit. We show results derived from pre-launch predictions and on-orbit solar diffuser collects. In this section we focus on the bolded outlined parts of the process illustrated in Figure 4a,b. While the pre-launch values for the solar diffuser data were based on the BATC processing system, to further enhance the confidence in the interpretation of on-orbit results, the raw OLI response to the sun-illuminated solar diffuser was converted to radiance using two independent processing systems, the USGS official Landsat Product Generation System (LPGS) processing and BATC processing. While both the USGS processing and BATC processing follow the same core steps, each has its own independently derived calibration parameters and non-linearity corrections. Furthermore, computation summaries for the on-orbit response will be shown for the first working panel solar diffuser collect on orbit and for the average of seven SD collects that occurred after the OLI approached a nominal response stability level. In all of the tables and plots in this section, the spectral radiance results are given in units of watt per meter squared per micrometer per steradian ( $W/m^2 sr \mu m$ ). All measured radiances reported (pre-launch or on orbit) are normalized to the earth–sun distance of 1 A.U. by multiplying the radiance by the earth–sun (E–S) distance square as known for each of the collect dates. The E–S distance is based on the cyclical earth–sun distance vs. DOY (day of the year) in A.U. units [24].

The results reported are organized into three parts that relate to the radiometric scale on-orbit revalidation. The first part is the comparison of the band average radiance response using the pre-launch-derived TOA-predicted radiance and the actual early evaluation for the TOA on orbit after all of the collects are normalized to 1[AU] earth–sun distance, accounting for the variations between the collects' dates (Tables 6–8). The second part checks the OLI TOA radiance response to the actual solar illumination diffuser panels against the predicted TOA response using the ChKur [25] and Thuillier [26] exo-atmospheric solar irradiance models (Tables 9–11). The reason for the use of these specific models is that ChKur was the long-term reference in the Landsat missions' vicarious calibration analysis and at the time Landsat 8 and Landsat 9 were built, the Thuillier model was the Committee on Earth Observation Satellites (CEOS) recommended reference solar irradiance spectrum model [27–29]. The last part of this results section shows the results for the TOA update to the reflectance conversion coefficients and comparison between the final on-orbit values and the pre-launch estimates (Table 12). While this part is not a critical element in the transfer to orbit, it is reported in this article for the reasons described in Section 2.

The radiance values shown in Table 6 include both the on-orbit results and the pre-launch estimates for TOA-predicted radiance. The pre-launch TOA-predicted radiance values were based on the working panel solar diffuser heliostat datasets taken in the two best test conditions collect dates. These were the key inputs for evaluating the agreements between the pre-launch and on-orbit results. As Figure 6 illustrates, the first two solar collects on orbit (depicted in the figure by the faded coloring) occurred when the OLI had not yet reached optimal on-orbit stability. This can be resolved in two possible methods. Option one, is to consider the trend-based correction as an additional stability error factor. This factor will be used to adjust the first collect date prior to assessing the impact of the transfer to orbit of the radiometric scale. The second option is to use the average of the seven working solar diffuser collects that span over the 36 days and that are taken after the OLI reaches nearly its nominal stability operations. As shown in Tables 7 and 8 we selected to show the results for both evaluation-method options. For Landsat 9 OLI, the near nominal stability operation was reached about 10 days after the initial turn-on. Table 6 lists the four types of measured results that illustrate results from the single first collect and the average of seven collects processed by each of the processing systems.

**Table 6.** Solar diffuser band average measured radiance pre-launch and on orbit. For the on orbit values, two options are shown.

Band Name	TOA-Predicted Radiance			On-Orbit Radiance [W/m <sup>2</sup> sr μm]		
	Image 1 BATC Processing Based on Heliostat Data 11/20/2018	Image 2 BATC Processing Based on Heliostat Data 12/14/2018	USGS Processing 10/30/2021	BATC Processing 10/30/2021	USGS Processing Average of Collects from 11/9/21–12/15/2021	BATC Processing Average of Collects from 11/9/21–12/15/2021
Coastal Aerosol	470.32	473.05	487.37	487.94	483.10	482.44
Blue	497.52	498.73	513.77	513.17	510.18	510.14
Green	465.2	465.46	479.03	480.41	477.29	477.49
Red	389.29	388.35	398.70	400.66	398.41	398.59
NIR	232.23	231.03	238.70	240.46	238.80	238.88
SWIR 1	59.407	59.139	61.130	61.516	61.199	61.179
SWIR 2	19.522	19.419	20.016	20.317	20.035	20.040
Pan	434.32	434.16	445.80	446.32	444.37	444.32

**Table 7.** Differences between TOA radiance 1st collect on 30 October 2021 and the predicted radiance.

Band Name	1st Solar Diffuser Collect % Difference from Predictions as (1-On-Orbit/Prediction) × 100 [%]				Expected 2-Sigma Uncertainty Levels [%]	
	Difference from Image 1 Prediction USGS Processing	Difference from Image 1 Prediction BATC Processing	Difference from Image 2 Prediction USGS Processing	Difference from Image 2 Prediction BATC Processing	On-Orbit Trend-Based Additional Stability Error in 1 <sup>st</sup> Solar Diffuser Collect	Heliostat-Based Prediction Uncertainty
Coastal Aerosol	−3.62	−3.75	−3.03	−3.15	0.91	6.48
Blue	−3.27	−3.15	−3.01	−2.90	0.73	5.74
Green	−2.97	−3.27	−2.91	−3.21	0.37	5.14
Red	−2.42	−2.92	−2.67	−3.17	0.07	4.26
NIR	−2.78	−3.54	−3.32	−4.08	0.05	4.16
SWIR 1	−2.90	−3.55	−3.37	−4.02	0.12	4.60
SWIR 2	−2.53	−4.07	−3.07	−4.62	0.11	4.80
Pan	−2.64	−2.76	−2.68	−2.80	0.33	5.08

**Table 8.** Best evaluation for differences between TOA radiance and predictions based on the radiance estimated from multiple datasets’ average responses shown in Table 6.

Band Name	Average <sup>a</sup> of Solar Diffuser Collects % Difference from Predictions as (1-On-Orbit/Prediction) × 100 [%]				Pre-Launch Heliostat Expected Uncertainty and Stability Measurement k = 2 [%]
	Difference from Image 1 Prediction USGS Processing	Difference from Image 1 Prediction BATC Processing	Difference from Image 2 Prediction USGS Processing	Difference from Image 2 Prediction BATC Processing	
Coastal Aerosol	−2.72	−2.58	−2.12	−1.98	6.48
Blue	−2.55	−2.54	−2.30	−2.29	5.74
Green	−2.60	−2.64	−2.54	−2.58	5.14
Red	−2.34	−2.39	−2.59	−2.64	4.26
NIR	−2.83	−2.86	−3.36	−3.40	4.16
SWIR 1	−3.02	−2.98	−3.48	−3.45	4.60
SWIR 2	−2.63	−2.65	−3.17	−3.20	4.80
Pan	−2.31	−2.30	−2.35	−2.34	5.08

<sup>a</sup> average excludes the 1st collect because the OLI did not reach nominal stability.

**Table 9.** Difference of pre-launch heliostat-based predictions from model-based predictions.

Band Name	E-Sun Model Computed Panel Radiance		Pre-Launch BATC Processing of Heliostat Test Data to Model % Differences as (1-Measured/Model_Prediction) × 100%			
	ChKur [W/m <sup>2</sup> sr μm]	Thuillier [W/m <sup>2</sup> sr μm]	Difference from Image 1 11/20/2018 to ChKur [%]	Difference from Image 2 12/14/2018 to ChKur [%]	Difference from Image 1 11/20/2018 to Thuillier [%]	Difference from Image 2 12/14/2018 to Thuillier [%]
Coastal Aerosol	469.83	471.48	−0.10	−0.68	0.25	−0.33
Blue	495.43	502.83	−0.42	−0.66	1.06	0.82
Green	466.35	458.55	0.25	0.19	−1.45	−1.51
Red	396.24	391.13	1.78	2.03	0.47	0.71
NIR	240.42	240.73	3.52	4.06	3.53	4.03
SWIR 1	62.15	63.48	4.62	5.10	6.42	6.85
SWIR 2	20.44	21.18	4.68	5.24	7.82	8.31
Pan	441.10	434.40	−1.56	−1.60	−0.02	−0.06

**Table 10.** Difference of actual TOA solar diffuser response and on-orbit model-based predictions.

Band Name	E-Sun Model Computed Panel Radiance		On-Orbit Average of Solar Diffuser Collects % Difference from Model as (1-On-Orbit/Model_Prediction) × 100%			
	ChKur [W/m <sup>2</sup> sr μm]	Thuillier [W/m <sup>2</sup> sr μm]	Difference from ChKur Predict USGS Processing [%]	Difference from ChKur Predict BATC Processing [%]	Difference from Thuillier Predict USGS Processing [%]	Difference from Thuillier Predict BATC Processing [%]
Coastal Aerosol	469.83	471.48	−2.82	−2.68	−2.46	−2.32
Blue	495.43	502.83	−2.98	−2.97	−1.46	−1.45
Green	466.35	458.55	−2.35	−2.39	−4.09	−4.13
Red	396.24	391.13	−0.55	−0.59	−1.86	−1.91
NIR	240.42	240.73	0.67	0.64	0.80	0.77
SWIR 1	62.15	63.48	1.54	1.57	3.60	3.63
SWIR 2	20.44	21.18	1.97	1.94	5.40	5.37
Pan	441.10	434.40	−0.74	−2.48	−0.72	−2.23

**Table 11.** The comparison of various residual difference and uncertainty factors related to the difference in model-based predictions in the pre-launch and the on-orbit evaluations.

Band Name	Pre-Launch Multi-Scenes Average of Heliostat to Model % Difference		Transfer to Orbit Computed Residual Uncertainty as $\sqrt{ (\text{on-orbit } \% \text{ Difference from Model}^2 - \text{Average Heliostat } \% \text{ Difference from Model}^2) } \times \text{Sign Correction to Match On-Orbit } \% \text{ Difference from Model of Table 10}$				Average of Computed Residual Transfer to Orbit Uncertainty Across both Processing Systems		Pre-Launch Heliostat Expected Uncertainty and Stability Measurement k = 2 [%]
	ChKur [%]	Thuillier [%]	USGS Processing to ChKur [%]	BATC Processing to ChKur [%]	USGS Processing to Thuillier [%]	BATC Processing to Thuillier [%]	ChKur [%]	Thuillier [%]	
Coastal Aerosol	−0.39	−0.04	−2.80	−2.65	−2.46	−2.32	−2.73	−2.39	6.48
Blue	−0.54	0.94	−2.93	−2.92	−1.12	−1.11	−2.92	−1.12	5.74
Green	0.22	−1.48	−2.34	−2.38	−3.81	−3.86	−2.36	−3.83	5.14
Red	1.91	0.59	−1.83	−1.81	−1.76	−1.81	−1.82	−1.79	4.26
NIR	3.79	3.78	3.73	3.74	3.69	3.70	3.74	3.70	4.16
SWIR 1	4.86	6.63	4.61	4.60	5.57	5.55	4.60	5.56	4.60
SWIR 2	4.96	8.06	4.56	4.57	5.99	6.01	4.56	6.00	4.80
Pan	−1.58	−0.04	−1.40	−1.92	−0.72	−2.23	−1.66	−1.48	5.08

Tables 7 and 8 are showing the evaluated changes in the on-orbit response relative to the pre-launch-based TOA predictions for each of the four on-orbit processed versions against each of the corresponding pre-launch reference collects. In the rightmost columns of Tables 7 and 8 we include the heliostat test configuration uncertainty two-sigma levels that the on-orbit changes need to be checked against. Uniquely for Table 7, due to the temporary added OLI instability error of the first collect, we included the per band additional estimated uncertainty associated with that collect. In Table 7, the comparison of the evaluated change impact is shown as a % relative to the pre-launch results. The values of these comparisons show that all bands and all processing systems results are under the  $k = 2$  heliostat collects uncertainty. While additional error due to the OLI first collect day instability can be considered for these datasets, it was not needed. When considering the results for the average response shown in Table 8, the variations in the results between the two independent processing systems for all bands agree within  $<0.15\%$ . In contrast, the comparisons that are based on a single collect, as seen in the results shown in Table 7, illustrate a larger mismatch between the processing systems. Comparing between the differences of the two pre-launch reference collect dates, we can see a difference of up to  $\sim 0.6\%$  between the two collects. The most likely reasoning for this level of difference is the uncertainty for the atmospheric transmission values derived. Accounting for such variation is included in the overall heliostat uncertainty budget. Examining the values of both Tables 7 and 8 while being conservative, we can state that the transfer to orbit based on the working solar diffuser results alone, shows a change impact level that is  $<3.9\%$  for all bands (excluding the Cirrus band). Since the level of  $3.9\%$  is less than the lowest heliostat  $k = 2$  uncertainty level, we can conclude that no significant change occurred on orbit. For all subsequent analysis steps discussed in this article that involved on-orbit data, we selected to use results from the multiple collects average TOA radiance response since these hold a reduced level of stability uncertainty.

In the second part of the solar diffuser response analysis, we show the comparison between the exo-atmospheric solar irradiance spectral models-based TOA predictions to both the pre-launch (Table 9) and on-orbit (Table 10) measured responses. Since the OLI radiance calibration path is separate from the reflectance calibration, we do not expect the radiance to agree with any model-based results within the heliostat uncertainty levels. A recent publication by Thuillier G. et al. also discussed variations between various solar irradiance models [30]. However, we do expect that the differences between the measured and models-based radiances to be maintained for both the pre-launch and on-orbit collects, at levels that are within the heliostat uncertainty. The comparison that tests this expected result is summarized in Table 11, and in that manner, it adds one more evaluation for the transfer-to-orbit-induced impact.

Table 9 shows the comparison of the two evaluated models to the two pre-launch heliostat collects as processed with the BATC processing system. Table 9 model-based values were computed based on the compilation of diffuser laboratory measured reflectance factors, the OLI final relative spectral response data, and the model spectral radiance. Table 9 results list the mismatch between the two models in each of the pre-launch collect dates as a percent change relative to the model-based predicted TOA values. The largest mismatch between the pre-launch measured values and the models-based TOA radiance occurred for the SWIR2 Thuillier model. This is expected since the baseline radiance and reflectance values from the NIST start with higher uncertainties for the SWIR spectral bands. Since all laboratory measurements that tie the reference calibration articles to the NIST scales occurred in ambient conditions, it is expected that for the SWIR bands the uncertainties grow. For ambient testing, it has been shown that the atmospheric path transmission induces higher uncertainties for radiance measurements in the NIR and SWIR spectral bands [20]. Water vapor and particle scatter are examples for some of the causes that impact these longer wavelengths signal losses. Examining the SWIR bands results for the ChKur model, Table 9 shows that at least one of the two heliostat collects matched the model-predicted results within the  $k = 2$  heliostat expected uncertainties.

Table 10 shows the collated summary for the evaluation of the average-based on-orbit solar diffuser response against the two solar irradiance spectral models. Compared to the pre-launch results in Table 9, Table 10 results demonstrate a better agreement between the on-orbit measurements and for both of the solar irradiance model-based predictions. Specifically, for the ChKur model, both processing systems showed the on-orbit measurements agreed at a level that is less than the  $k = 2$  heliostat measurement uncertainty and nearly approach the direct OLI reflectance scale uncertainty (Table 3). Comparing between the results for each of the models, in Table 10 both processing systems show the same differences vs. spectral band signature seen with the pre-launch heliostat results. The worst band was, again, the SWIR2 with a difference of nearly 3.4% between the two models.

Table 11 bolded values columns on the right side illustrate the change in the assessment from the TOA model-based predictions. In a way, these values can be interpreted as the model-based assessments for the transfer-to-orbit impact. The values shown summarize the per model results derived per band from the average of both processing systems, and the assessed changes from pre-launch to on orbit. In the two leftmost columns of Table 11, we summarize Table 9 pre-launch results as an average per model from the two pre-launch observations. These pre-launch average values are the reference values that the on-orbit results from Table 10 are compared against. The sign of the model-based transfer-to-orbit impact is forced to match the sign seen in the Table 10 on-orbit values. These results again illustrate that the SWIRS bands are suspected to have the largest impact. When examining the results closer, we can see that these are impacted mainly by that large mismatch to the models in the pre-launch data and the larger model-specific uncertainties.

In the last and third part of the diffuser-based observations, updated TOA on-orbit measured radiance were used from both the working and the pristine diffusers to replace the estimated pre-launch predicted values. This leads to an update for the reflectance conversion factors, which, like the absolute calibration gain parameters, are a set of band average values. While a quick on-orbit update can be made as early as 46 days after turn-on, the actual official on-orbit value for this parameter was evaluated towards the end of the commissioning period. This way, we follow the same process made for Landsat 8 that allows the evaluation of both working and pristine solar diffuser reflectance panels. This allowed us to obtain a larger set of datapoints and to compute the values after all additional relative gains and other gain refinements had been applied. Some of the radiometric adjustments applied were the gain updates that aimed to cross-calibrate the radiometric scales of Landsat 8 and Landsat 9. In addition, during the end of the commissioning period, unlike during the early orbit operation, the spacecraft follows the WRS-2 ground track after it reached its final orbit altitude and all on-orbit calibration collect sequences follow a pre-scheduled cycle. The combined effect of these aids the OLI in reaching a plateau in its level of radiometric response stability. In Table 12, the change applied to the radiance to reflectance conversion factors between the pre-launch and on orbit states is shown along with the actual parameter values. This table illustrates that the updates made are still within the expected transfer-to-orbit known uncertainty and the two-sigma total radiometric scale uncertainties. The data reveal that the largest update was in the Cirrus band with 9.37%, and the second largest was for the Green band, with  $-5.17\%$ . For the Green band, the two-sigma combined heliostat/heliostat expected uncertainty and stability error was 5.51% (Table 7). This illustrates that the Green band, even after all gain updates are included, still re-validates its pre-launch calibration within the expected uncertainty levels. The negative value means the radiance measured on orbit was higher than expected pre-launch. At the same time, the Cirrus band that had no gain updates at the end of the commissioning resulted in a change value of 9.37%, which is approaching the two-sigma limit of the system performance requirement. The solar diffuser data alone cannot confirm if this level of change is due to actual transfer-to-orbit impact or an error made in the assigned pre-launch calibration radiance gain parameters. The question related to the transfer-to-orbit impact on the Cirrus band is resolved in the next section, where we use the stimulation lamp datasets. The root cause for the observed change was not

resolved until we obtained more joint solar and lunar on-orbit data with both Landsat 8 and Landsat 9 systems. Ultimately, follow-on investigation and data analysis through the first year of on-orbit operation revealed the root cause to be an error in the applied pre-launch gain parameter that resulted in applying a wrong pre-launch radiance scale. After the mistake was corrected by applying the correct pre-launch parameters to the USGS processing, which adjusted the absolute radiance scale for the Cirrus band, it was confirmed that the pre-launch to on-orbit change in the reflectance factor variation dropped to a level of 3.32%, which is close to the results computed for other OLI spectral bands, and the new update level is within the two-sigma uncertainty limit confirmation range. Please note that, due to this planned, early on-orbit update to the reflectance conversion factors, the Cirrus band radiance scale error did not impact the uncertainty level of early released USGS TOA reflectance science products.

**Table 12.** End of OLI commissioning period Radiance to Reflectance conversion factors Compared to Pre-launch estimates. The units for the conversion factors are  $[m^2 \times sr \times \mu m/W]$  as they are described in the CPF configuration control document [31].

Band Name	TOA Radiance to Reflectance Conversion Factor		On-Orbit Update Change as (1-On-Orbit/Pre-Launch) $\times$ 100 [%]
	Pre-Launch [ $m^2 \text{ sr } \mu m/W$ ]	On-Orbit Update [ $m^2 \text{ sr } \mu m/W$ ]	
Coastal Aerosol	0.00153916	0.00159491	−3.62
Blue	0.00147994	0.00155286	−4.93
Green	0.00160683	0.00168997	−5.17
Red	0.00193829	0.00199388	−2.87
NIR	0.00326860	0.00324993	0.57
SWIR 1	0.01304526	0.01300925	0.28
SWIR 2	0.03857498	0.03852789	0.12
Pan	0.00173765	0.00176143	−1.37
Cirrus	0.00864384	0.00783421	9.37

### 3.3. Simulation Lamp Color Temperature Analysis and Validation of Cirrus Band Transfer-to-orbit Performance

In this section, the results of pre-launch color temperature (CT) model fit parameters and residual error are used to compute updated on-orbit color temperature model results. Since Section 3.2 confirmed that no credible change occurred throughout the launch, the processing of stim lamp data used the same pre-launch calibration parameters to convert the OLI digital counts response to calibrate radiance response. The residual CT model error computed relative to pre-launch measurements aimed to minimize the error among all spectral bands. The residual error was computed as a relative error to the model-based response (i.e., gain error); this way, when a model-based update is made on orbit (finding the new color temperature fit), the pre-launch-based relative residual error correction can be applied to the new color temperature illumination. The assumption that the model error is going to remain the same for both on orbit and pre-launch was rooted in the fact the light bulbs used the transmission of the system and the responses all remained invariant within the expected uncertainties. An error in that assumption may result in additional residual difference between the stim lamp-based and the solar diffuser-based paths for the assessment of the transfer-to-orbit impact. Such additional error terms can be considered a systematic error that accounts for several changes that occur in the stim lamp operations that are not accounted for by the model fit parameters. This leads to an extra correction mainly due to changes in the stim lamp system rather than in the OLI FPA response. Based on experience with the stim lamp on-orbit operation of Landsat 8 OLI, the SL source was expected to mainly have an impact to its modeled color temperature and associated transmission scaling parameters. However, an additional adjustment to the pre-launch residual error may be needed if the CT gap is large. Lastly, we report, for all spectral bands, the comparison between the computed and readjusted model radiance to

OLI direct on-orbit calibrated radiance response. From this summary comparison, the most important output is the value computed for the Cirrus band.

The Landsat 9 OLI stim lamp subsystem is identical in design to that of the Landsat 8 OLI stim lamp. Both systems use tungsten-halogen bulbs that illuminate the full focal plane while passing through the entire telescope subsystem and produce a non-uniform signal. The main difference between Landsat 8 and Landsat 9 is in the different lamp pairs that are being turned on together, producing different illumination patterns on the focal plane (Figure 1). This alone is a strong demonstration for the dependence of the signal profiles, and the spectral throughput of the stim lamp system, on the physical position of the bulb relative to the stim lamp diffuser. Furthermore, we know that the filament sag position is another factor that impacts the SL power output. However, as seen throughout the pre-launch testing, each fixed configuration stim lamp demonstrated pre-launch stability and repeatability performance on the order of  $<0.5\%$ , with a two-sigma worst case (Figure 8). Therefore, the stim lamp can be used to monitor the band average response both on orbit and pre-launch, mimicking a secondary calibration reference that is stable and sensitive enough to validate the impact of the transfer to orbit. During pre-launch radiometric scale realization, the calibration of the stim lamp response was tied to our primary radiance-integrating sphere reference. On orbit, while using the same pre-launch calibration parameters, we evaluated the stim lamp response in comparison to the OLI working solar diffuser panel. That serves as the solar-illuminated on-board NIST traceable absolute reflectance calibration reference.

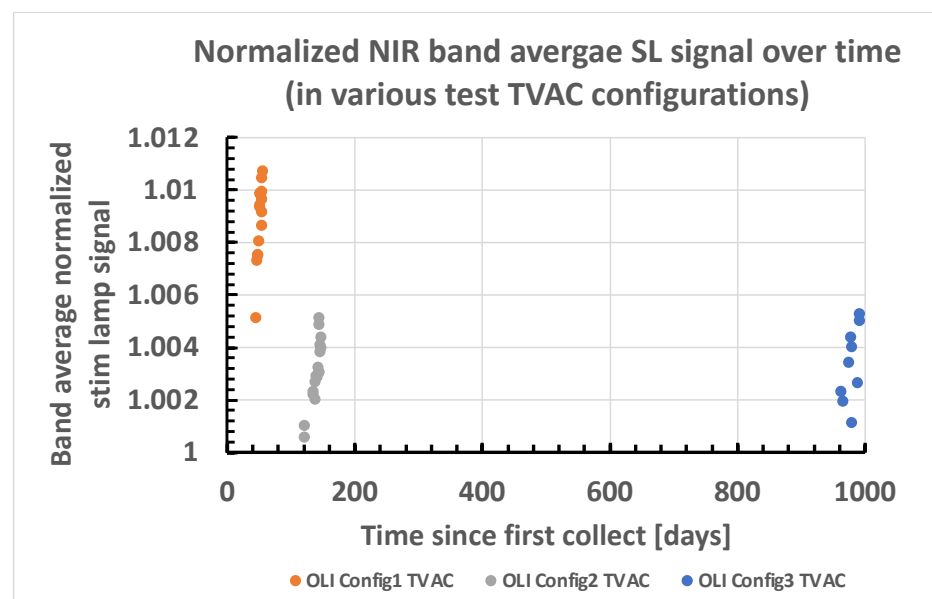


**Figure 8.** NIR band average pre-launch working SL net signal response stability over a range of simulated on-orbit conditions and over time as tested during three thermal-vacuum chamber (TVAC) configurations with primary electronic side. Illustrating a stability at the level of, or better than,  $0.5\%$ , two sigma within each of the test configurations. Each set of collect data shown is for the 1.8 sec average response post the warmup duration of 2.67 min.

The spectral information about the working lamp is summarized in a three-part fit model that includes an effective color temperature, a scaling factor, and residual error for the modeled fit. The model is based on the blackbody plank-function radiance for a body at a temperature set by the CT model parameter. The model is scaled by the scaling factor and lastly the residual error between the measured and the modeled radiance for a fixed CT value is computed. The process for determining the optimal CT parameter for the lamp is an iterative numerical evaluation. Excluded from the computation was the Pan band, as it is a wide spectral response band that will not fit the task of finding the best fit spectral

signature. The final CT set per detector was the mean value of two estimates for the optimal fit that aimed to both balance the error among all narrow spectral bands and minimize it. Lastly, to minimize the variability and uncertainty in the derived final CT fit values, for each spectral band, the data used for the fit involved the zone of detectors that were near the peak SL signal. The mean results from multiple collects for each test configuration were used to determine the final CT model fit values. Using this fixed CT value, we computed the new per detector scaling factor and the associated residual error parameters. Pre-launch we had three stim lamp configurations: two during instrument level testing TVAC and one during the spacecraft TVAC configuration. The color temperature fit model and the residual error in all eight bands (excluding the Pan band) were computed for all data collects and are listed in Tables 13 and 14. For each configuration, three collects from different days were evaluated to understand the analysis and stim lamp stability impacts on the results.

In Table 13, each set of TVAC testing configuration results includes a summary for the mean and variance values for the CT temperature as well as the residual error. The last bolded line in Table 13 lists the summary of the overall baseline residual error from the pre-launch that was then used during the on-orbit processing analysis (i.e., the green outlined frame in Figure 4b). Table 14 lists the on-orbit SL model fit results after applying the pre-launch expected residual error. The last two bolded lines in this table show the final estimates of the impact of the TTO on the OLI as derived from the SL-based assessments. The data shown sampled both early collect days in 2021 that included DOY 304, 326, and 338, as well as collects taken once we were in the final orbit position that included, in 2021, DOY 345 and, in 2022, DOY 36 and 132. Like in the pre-launch summaries per configuration, the on-orbit results were collated to mean and variance values. After the SL to SD error matching adjustment to the SL model fit, the residual error was applied by adding 13% to the per band mean residual error, and the results are shown in a bolded line of Table 14. These values represent the estimated net OLI TTO impact as evaluated with the SL collects. The associated estimates for the  $k = 2$  uncertainty in the SL-based assessment were mainly impacted by the SL to SD adjustment that its root cause linked to the SL operational change. In pre-launch, the CT change among the various configurations was less than the 6K shift to on orbit causing the SL to change its effective CT by nearly 50K. Still, the within configuration-derived stability for the CT and the residual errors were just as good, if not even better, on orbit, when compared to the pre-launch values. The results, as illustrated in Table 14 and Figure 9, highlight that the Cirrus band residual error, which was derived from the stim lamp analysis, is in the same family as the other spectral bands. Hence, this leads to the re-confirmation that the Cirrus band radiance scale established during pre-launch is still valid within the expected band measurements uncertainties.

In Table 14, the adjusted on-orbit stim lamp-based transfer-to-orbit residual fit error of the Cirrus band resulted in a value of 0.98%. When accounting for the pre-launch variability in the residual error and the stim lamp stability, this results in a worst-case estimate for this band that can reach the level of 1.8%, which is still within the radiometric uncertainty error bar reach, and that can cross the 0% change line. The stim lamp path to revalidating the radiance scale worked well due to the ability to relate the SL results to solar diffuser-based analysis.

**Table 13.** Pre-launch CT model fit results for all evaluated spectral bands.

pre-Launch Stim Lamp Collects Date and Configuration and Summaries	Color Temperature Computed [K]	Residual Error Computed from Scaled Color Temperature Model Fit to Measured SL Response [%]							
		Coastal Aerosol	Blue	Green	Red	NIR	Cirrus	SWIR 1	SWIR 2
Sept 4 2018—config 1	2815.86	11.3	17.5	8.9	12.1	18.8	−4.0	5.7	25.8
Sept 5 2018—config 1	2814.79	11.3	17.4	8.7	12.0	18.8	−3.8	6.0	26.1
Sept 6 2018—config 1	2816.49	11.2	17.6	8.9	12.1	18.8	−4.0	5.7	25.7
config 1 mean results summary	2815.71	11.3	17.5	8.8	12.1	18.8	−3.9	5.8	25.9
config 1 variance results summary	1.70	0.1	0.2	0.2	0.1	0.0	0.2	0.2	0.3
Dec 3 2018—config 2	2810.92	11.2	17.6	8.9	12.0	18.7	−3.9	5.8	25.9
Dec 5 2018—config 2	2810.72	11.3	17.6	8.7	11.9	18.6	−3.9	5.8	25.9
Dec 7 2018—config 2	2809.70	11.2	17.3	8.9	11.9	18.8	−3.6	6.2	26.4
config 2 mean results summary	2810.45	11.2	17.5	8.8	11.9	18.7	−3.8	5.8	26.1
config 2 variance results summary	1.22	0.2	0.3	0.2	0.1	0.1	0.3	0.4	0.5
Mar 27 2018—config 3	2810.14	11.1	17.6	8.9	12.1	18.7	−3.7	5.8	25.7
Mar 17 2018—config 3	2810.71	11.2	17.6	8.9	12.1	18.6	−4.0	5.7	25.4
Mar 27 2018—config 3	2811.18	11.2	17.6	8.9	12.1	18.7	−4.0	5.7	25.5
config 3 mean results summary	2810.68	11.2	17.6	8.9	12.1	18.7	−4.0	5.7	25.5
config 3 variance results summary	1.04	0.1	0.1	0.0	0.0	0.1	0.1	0.1	0.2
Baseline residual error for use with on-orbit data		11.2	17.5	8.8	12.0	18.7	−3.9	5.8	25.8

**Table 14.** On-orbit CT model fit results and final summary after applying all adjustments for all evaluated spectral bands.

On-Orbit Stim Lamp Collects Dates and Summaries	Color Temperature Computed [K]	Residual Error Computed from Scaled Color Temperature Model Fit to Measured SL Response with Applied Pre-Launch Baseline Residual Correction Adjustments [%]							
		Coastal Aerosol	Blue	Green	Red	NIR	Cirrus	SWIR 1	SWIR 2
Oct 31 2021	2862.88	−15.4	−15.7	−14.6	−15.0	−15.5	−12.0	−13.0	−15.5
Nov 22 2021	2862.75	−15.2	−15.7	−14.6	−15.0	−15.6	−12.0	−13.1	−15.5
Dec 4 2021	2863.36	−15.2	−15.7	−14.6	−15.0	−15.5	−12.0	−13.0	−15.5
Dec 11 2021	2862.14	−15.0	−15.7	−14.6	−15.1	−15.6	−12.0	−13.0	−15.5
Feb 5 2022	2862.63	−15.0	−15.7	−14.6	−15.1	−15.6	−12.0	−13.0	−15.4
May 12 2022	2862.88	−15.0	−15.7	−14.6	−15.0	−15.6	−12.0	−13.0	−15.5
On-Orbit mean results summary	2862.77	−15.1	−15.7	−14.6	−15.0	−15.6	−12.0	−13.0	−15.5
On-Orbit variance results summary	1.22	0.4	0.0	0.0	0.1	0.1	0.0	0.1	0.1
SL to SD Residual TTO error additional model fit adjustments		13.0	13.0	13.0	13.0	13.0	13.0	13.0	13.0
Adjusted On-orbit stim lamp TTO residual error summary		−2.14	−2.71	−1.59	−2.02	−2.57	0.98	−0.04	−2.48
Stim lamp-based TTO results uncertainty k = 2		13.5	13.4	13.3	13.3	13.3	13.8	13.4	13.5

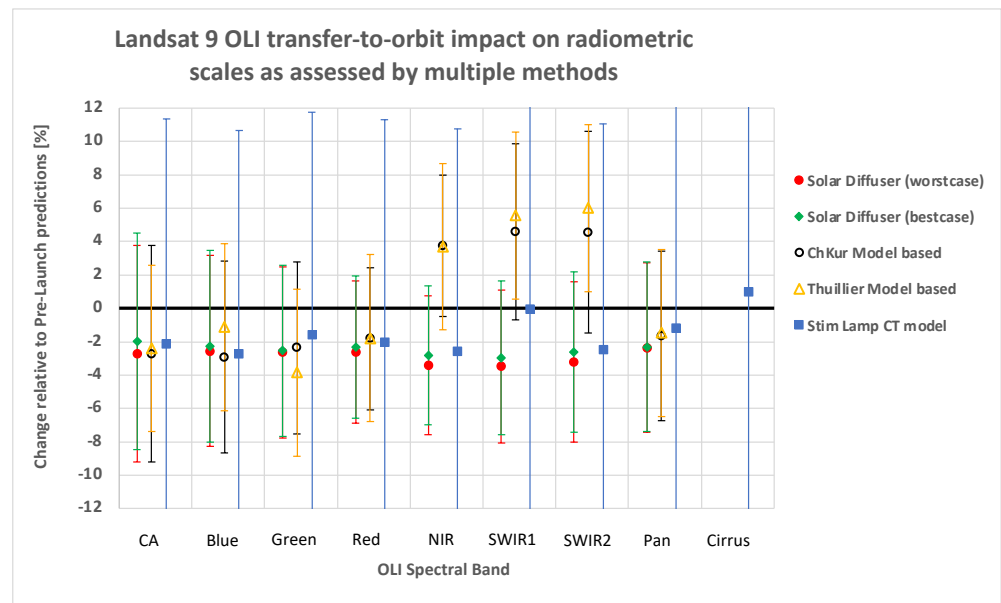


**Figure 9.** Estimated OLI radiometric scale impact due to the transfer to orbit using solar diffuser, models-based and stim lamps CT model results as shown in the tables above. Values are shown with associated expected  $k = 2$  uncertainty level shown by the error bars (The negative values mean that on-orbit response was higher than predicted). Stim lamp-based results display a  $\sim 13.4\%$  error bar due to the applied adjustment between pre-launch and on orbit. Also, the NIR, SWIR1 and SWIR2 error bars are adjusted to account for the inherent model-to-NIST calibration mismatch that is not related to TTO.

In Figure 9, all of the results from methods used in this article for the revalidation of the radiometric scales for all bands are shown together with the associated  $k = 2$  uncertainties in each, depicted by the error bars. The solar diffuser best and worst values in Figure 9 are showing the estimates computed by two independent processing systems in reference to two collect dates. The error bars from all bands and methods, except for the SWIR1 and SWIR2 model-based results from the Thuillier model, cross the plot's 0% change line. This affirms that the transfer to orbit via the launch event did not change the absolute radiometric scale at a level beyond the expected uncertainties, hence it can be considered the same as had been established pre-launch. In Figure 9, the model-based NIR and SWIR band results show a positive error sign rather than the negative errors seen with the SL and SD-based analysis. The positive values in this plot mean that the NIR and SWIR band on-orbit responses were lower than the model predicts. Table 11 Thuillier model-based results show that, for these spectral bands, the pre-launch heliostat results carry most of the cause for the higher transfer-to-orbit impact estimate. The direct on-orbit results in Table 10 illustrate that only the SWIR2 band resulted in a measured error that was larger than the expected  $k = 2$  error bars.

#### 4. Conclusions

The revalidation of the absolute radiance scale calibration of the OLI was conducted successfully during the early commissioning period of Landsat 9. On-orbit analysis results demonstrated that several values that are contributing terms to the radiance and reflectance radiometric scale uncertainties met the predicted uncertainty allocations. Shortly after launch, the calibration team of the Landsat 9 concluded that no updates were necessary for the absolute radiometric scales of the Landsat 9 OLI. This conclusion is illustrated and supported by Figure 9, which shows how all transfer-to-orbit evaluation methods used by the process (Figure 4) cross the 0% change line when considering the expected uncertainties of each method. While the stim lamp path to radiance scale revalidation required a 13% systematic model correction, in all spectral bands the post correction agreements of the SL

results with the 0% change line were within the OLI  $k = 2$  radiance calibration uncertainty (Table 2). Therefore, using the original pre-launch radiometric calibration parameters was a sufficient starting point for producing quality Landsat science products. Two main paths that assisted in evaluating the transfer to orbit for Landsat 9 OLI involved the solar diffuser collects and on-board stim lamp collects. These collects and the follow-up analysis duplicated methods that were applied during the Landsat 8 transfer to orbit. During the analysis conducted for the transfer to orbit, the team noted the positive impacts of the improved pre-launch calibration work of Landsat 9 OLI and the assistance provided by the availability of ground system processing tools that were available during the early commissioning period. As expected, the final radiance to reflectance conversion factors had been set based on the on-orbit collects that occurred in the commissioning period. The processing tools that were available at the time of commissioning played a supporting role in enabling a quick turnaround of analysis reports and independent validations of allocated uncertainties to the radiometric scales. The main challenge in the radiance scale validation was related to the Cirrus band, which did not have sun-illuminated pre-launch collects. This was mitigated by using the stim lamp as a secondary radiance calibration source to validate that no impact to the radiometric scale occurred at launch. The approach that links the solar diffuser results of the transfer to orbit to the stim lamp-based results is a unique process for OLI radiance scale revalidation. It highlights an additional approach that can supplement the missing information for spectral bands that cannot be directly evaluated with the solar diffuser panel data. While the analysis for the Cirrus band transfer to orbit confirmed no change occurred to the OLI response post launch, within the first year of on-orbit operation it was confirmed that the applied Cirrus band radiance gain parameters in the official USGS processing system were applying a wrong pre-launch absolute gain parameter. After this parameter correction, the residual update of the reflectance conversion factor for the Cirrus band was in family and within the same expected uncertainty levels as for all other OLI spectral bands. The repeated success in the transfer-to-orbit results for the OLI systems in both Landsat 9 and Landsat 8 is a testament to a robust design for the integration and testing plan conducted pre-launch, which included the radiometric-scale definitions as well as stability assessments that considered contamination control, vibrations, and the application of lessons from Landsat 8. When evaluating the transfer to orbit for the Landsat 9 OLI, numerous datasets were used. While these datasets are a limited, small sample of data, they are well-controlled sets that enabled the revalidation of the radiometric scale at an operational period that is very dynamic from the mission point of view. In this dynamic period the OLI system was on the path to reaching its steady state radiometric response stability. Examining long-term trend plots, which are part of the USGS quarterly calibration reports [32], shows that the data collected following a turn-on of the system followed an expected response change pattern that was nearly the same for both Landsat 8 and Landsat 9 (Landsat 9 has been added to the quarterly reports only, since the 2023 third quarter is expected to be released soon by USGS). The main difference is that Landsat 9 exhibits a shorter duration in reaching this steady state in radiometric stability. While the activity done during the transfer to orbit provided an initial validation to the calibration scale, for the OLI, the CalVal team used this just as a starting point to further refine and update the radiometric scales of the mission with follow-on activity that utilized vicarious calibration and cross-calibration checks against comparable earth observing systems.

**Author Contributions:** All of the authors were involved in the various aspects of the radiometric scale assessment pre-launch and on orbit. R.L.; writing and transfer-to-orbit analysis both of heliostat data and Lamp Color Temperature modeling analysis. B.L.M. and K.J.T.; NASA Landsat CalVal managers, reviewed the analysis results and guided the team during the commissioning period. R.L., J.A.B. and J.A.M.; processed the OLI data and conducted radiometric characterization, involving the reflectance conversion factors and stim lamp and solar diffusers datasets processing and noise analysis. All authors have read and agreed to the published version of the manuscript.

**Funding:** This research received no external funding.

**Data Availability Statement:** The data presented in this study are available in article as well as referenced websites. Parts of the data shown related to OLI2 calibration source collects is only available on request due to restrictions.

**Acknowledgments:** The authors extend special thanks to Geir Kavarn, Sandra Collins, and Jordan Marks from Ball Aerospace & Technologies Corp for performing calibration and data analysis for the OLI instrument during the pre-launch and on orbit, resulting in many of the reports related to the pre-launch established radiometric scale, including an independent analysis for transfer-to-orbit results and assessment of the various test configurations-associated uncertainties. As described, the approach for the evaluation of the transfer-to-orbit uncertainties shown in this paper is built on base methodology that these BATC calval team members developed. The authors extend special thanks to Jeffrey Czapla-Myers from Remote Sensing Group, Wyant College of Optical Sciences in the University of Arizona for explaining the heliostat analysis involved with the heliostat collects test conditions, and the associated steps involving the MODTRAN radiative transfer tool. The authors extend special thanks to Obaidul Haque from the USGS Landsat EROS calval team for reviewing the plots related to the SNR changes between pre-launch and on orbit. Please note that any use of trade, firm, or product names is for descriptive purposes only and does not imply endorsement by the U.S. Government. The authors will like to also thank the USGS flight operation team for their support in conducting all of the on-orbit operations as requested by the calibration validation team. The flight operation team effort enabled the production of the datasets needed for the analysis conducted in this article.

**Conflicts of Interest:** Authors Raviv Levy, Jeffrey A. Miller, Julia Barsi were employed by the company Science Systems and Applications, Inc. All authors declare no conflict of interest.

## References

1. Pearlman, A.; Efremova, B.; Montanaro, M.; Lunsford, A.; Reuter, D.; McCorkel, J. Landsat 9 Thermal Infrared Sensor 2 On-Orbit Calibration and Initial Performance. *IEEE Trans. Geosci. Remote Sens.* **2022**, *60*, 1002608. [CrossRef]
2. Cao, C.; De Luccia, F.J.; Xiong, X.; Wolfe, R.; Weng, F. Early On-Orbit Performance of the Visible Infrared Imaging Radiometer Suite Onboard the Suomi National Polar-Orbiting Partnership (S-NPP) Satellite. *IEEE Trans. Geosci. Remote Sens.* **2014**, *52*, 1142–1156. [CrossRef]
3. Lachérade, S.; Lonjou, V.; Farges, M.; Gamet, P.; Marcq, S.; Raynaud, J.-L.; Trémas, T. Sentinel-2 radiometric image quality commissioning: First results. In Proceedings of the SPIE 9639, Sensors, Systems, and Next-Generation Satellites XIX, Toulouse, France, 12 October 2015; p. 963905. [CrossRef]
4. Micijevic, E.; Haque, M.O.; Barsi, J.A.; Levy, R.; Anderson, C.; Thome, K.; Gross, G.; Czapla-Myers, J. Landsat 9 Operational Land Imager On-orbit Radiometric Performance. *Remote Sens.* **2024**, *in review*.
5. Czapla-Myers, J.S.; Thome, K.J.; Anderson, N.J.; Leigh, L.M. Cibebe Teixeira Pinto and Brian N. Wenny The Ground-Based Absolute Radiometric Calibration of the Landsat 9 Operational Land Imager. *Remote Sens.* **2024**, *16*, 1101. [CrossRef]
6. Kaewmanee, M.; Leigh, L.; Shah, R.; Gross, G. Inter-Comparison of Landsat-8 and Landsat-9 during On-Orbit Initialization and Verification (OIV) Using Extended Pseudo Invariant Calibration Sites (EPICS): Advanced Methods. *Remote Sens.* **2023**, *15*, 2330. [CrossRef]
7. Gross, G.; Helder, D.; Leigh, L. Extended Cross-Calibration Analysis Using Data from the Landsat 8 and 9 Underfly Event. *Remote Sens.* **2023**, *15*, 1788. [CrossRef]
8. Malone, K.J.; Schrein, R.J.; Bradley, M.S.; Irwin, R.; Berdanier, B.; Donley, E. Landsat 9 OLI 2 focal plane subsystem: Design, performance, and status. In Proceedings of the SPIE 10402, Earth Observing Systems XXII, San Diego, CA, USA, 5 September 2017; p. 1040206. [CrossRef]
9. Knight, E.J.; Kvaran, G. Landsat-8 Operational Land Imager Design, Characterization and Performance. *Remote Sens.* **2014**, *6*, 10286–10305. [CrossRef]
10. Markham, B.; Barsi, J.; Kvaran, G.; Ong, L.; Kaita, E.; Biggar, S.; Czapla-Myers, J.; Mishra, N.; Helder, D. Landsat-8 Operational Land Imager Radiometric Calibration and Stability. *Remote Sens.* **2014**, *6*, 12275–12308. [CrossRef]
11. Kvaran, G. Pre-launch Radiometric Characterization of the Operational Land Imager 2 (OLI 2). Spotlight Session: OLI, 2019 CALCON Technical Meeting 2019. Available online: <https://digitalcommons.usu.edu/cgi/viewcontent.cgi?article=1346&context=calcon> (accessed on 20 January 2024).
12. Markham, B.L.; Dabney, P.W.; Murphy-Morris, J.E.; Pedelty, J.A.; Knight, E.J.; Kvaran, G.; Barsi, J.A. The landsat data continuity mission operational land imager (OLI) radiometric calibration. In Proceedings of the 2010 IEEE International Geoscience and Remote Sensing Symposium, Honolulu, HI, USA, 25–30 July 2010; pp. 2283–2286. [CrossRef]
13. Patrick, H.J.; Cooksey, C.C.; Germer, T.A.; Nadal, M.E.; Zarobila, C.J. Bidirectional reflectance capabilities of the NIST Robotic Optical Scattering Instrument. *Appl. Opt.* **2021**, *60*, 8774–8786. [CrossRef] [PubMed]
14. Facility for Spectroradiometric Calibrations (FASCAL). Available online: <https://www.nist.gov/laboratories/tools-instruments/facility-spectroradiometric-calibrations-fascal> (accessed on 20 January 2024).

15. Yoon, H.W.; Proctor, J.E.; Gibson, C.E. FASCAL 2: A New NIST Facility for the Calibration of the Spectral Irradiance of Sources. In *Metrologia*; 2003; 40, pp. S30–S34. Available online: [https://tsapps.nist.gov/publication/get\\_pdf.cfm?pub\\_id=841660](https://tsapps.nist.gov/publication/get_pdf.cfm?pub_id=841660) (accessed on 20 January 2024). [[CrossRef](#)]
16. Levy, R.; Markham, B.L. Landsat 9 Operational Land Imager2 (OLI2) enhanced on-orbit linearity characterization. In Proceedings of the Landsat Earth Observing Systems XXVI, San Diego, CA, USA, 10 August 2021; Volume 11829, p. 118290K. [[CrossRef](#)]
17. Barsi, J.A.; McCorkel, J.; McAndrew, B.; Zukowski, B.; Shuman, T.; Johnston, S.; Markham, B. Spectral testing of the Landsat-9 OLI-2 instrument using the Goddard Laser Absolute Measurement of Radiance (GLAMR). In Proceedings of the SPIE 10764, Earth Observing Systems XXIII, San Diego, CA, USA, 7 September 2018; p. 1076405. [[CrossRef](#)]
18. Markham, B.; Barsi, J.A.; McCorkel, J.; McAndrew, B.; Pedelty, J. Spectral Response Characterization of the Landsat 9 Operational Land Imager 2 using the Goddard Laser for Absolute Measurement of Radiance (GLAMR). Spotlight Session: OLI, 2019 CALCON Technical Meeting. Available online: <https://digitalcommons.usu.edu/cgi/viewcontent.cgi?article=1350&context=calcon> (accessed on 20 January 2024).
19. LSDS-1574\_L8\_Data\_Users\_Handbook-v5.0 NOVEMBER 27, 2019. Available online: <https://www.usgs.gov/landsat-missions/landsat-8-data-users-handbook> (accessed on 20 January 2024).
20. Butler, J.; Brown, S.; Saunders, R.; Johnson, B.; Biggar, S.; Zalewski, E.; Markham, B.; Gracey, P.; Young, J.; Barnes, R. Radiometric Measurement Comparison on the Integrating Sphere Source Used to Calibrate the Moderate Resolution Imaging Spectroradiometer (MODIS) and the Landsat 7 Enhanced Thematic Mapper Plus (ETM+). *J. Res. (NIST JRES)* **2003**, *108*, 199–228. [[CrossRef](#)]
21. The MODTRAN®(MODerate Resolution Atmospheric TRANsmission) Computer Code. Available online: <http://modtran.spectral.com/> (accessed on 20 January 2024).
22. Levy, R.; Markham, B.L. Landsat 9 Operational Land Imager2 (OLI2) diffuser panel response lab predictions vs. pre-launch measurements. In Proceedings of the SPIE 11501, Earth Observing Systems XXV, Online, 17 September 2020; p. 115010P. [[CrossRef](#)]
23. Levy, R.; Miller, J.; Thome, K.J. Landsat 9 Operational Land Imager2 (OLI2) on-orbit results of new special characterizations. In Proceedings of the SPIE 12232, Earth Observing Systems XXVII, San Diego, CA, USA, 30 September 2022; p. 122320X. [[CrossRef](#)]
24. Landsat 8–9 Calibration Parameter File DATA FORMAT CONTROL BOOK-LSDS-1834 Version 3. Available online: <https://www.usgs.gov/media/files/landsat-8-9-calibration-parameter-file-dfcb> (accessed on 20 January 2024).
25. Chance, K.; Kurucz, R.L. An improved high-resolution solar reference spectrum for earth’s atmosphere measurements. *J. Quant. Spectrosc. Radiat. Transf.* **2010**, *111*, 1289–1295. [[CrossRef](#)]
26. Thuillier, G.; Hersé, M.; Labs, D.; Foujols, T.; Peetermans, W.; Gillotay, D.; Simon, P.C.; Mandel, H. The Solar Spectral Irradiance from 200 to 2400 nm as Measured by the SOLSPEC Spectrometer from the Atlas and Eureca Missions. *Sol. Phys.* **2003**, *214*, 1–22. [[CrossRef](#)]
27. Reference Solar Irradiance Spectrum Discussion Slides by Nigel Fox. Available online: [https://ceos.org/document\\_management/Working\\_Groups/WGCV/Meetings/WGCV-42/Presentations/Day%203/15\\_Reference%20Solar%20Irradiance%20spectrum%20wgcv42.pptx](https://ceos.org/document_management/Working_Groups/WGCV/Meetings/WGCV-42/Presentations/Day%203/15_Reference%20Solar%20Irradiance%20spectrum%20wgcv42.pptx) (accessed on 20 January 2024).
28. CEOS Reference Solar Irradiance Spectrum. Available online: <https://calvalportal.ceos.org/web/guest/solar-irrad-spectrum> (accessed on 20 January 2024).
29. Li, F.; Jupp, D.L.B.; Markham, B.L.; Lau, I.C.; Ong, C.; Byrne, G.; Thankappan, M.; Oliver, S.; Malthus, T.; Fearn, P. Choice of Solar Spectral Irradiance Model for Current and Future Remote Sensing Satellite Missions. *Remote Sens.* **2023**, *15*, 3391. [[CrossRef](#)]
30. Thuillier, G.; Zhu, P.; Snow, M.; Zhang, P.; Ye, X. Characteristics of solar-irradiance spectra from measurements, modeling, and theoretical approach. *Light Sci. Appl.* **2022**, *11*, 79. [[CrossRef](#)]
31. Earth Sun Distance Astronomical Units for Days of the Year. Available online: <https://www.usgs.gov/media/files/earth-sun-distance-astronomical-units-days-year> (accessed on 20 January 2024).
32. Landsat Calibration and Validation | U.S. Geological Survey-USGS. Available online: <https://www.usgs.gov/calval/landsat-calibration-and-validation> (accessed on 20 January 2024).

**Disclaimer/Publisher’s Note:** The statements, opinions and data contained in all publications are solely those of the individual author(s) and contributor(s) and not of MDPI and/or the editor(s). MDPI and/or the editor(s) disclaim responsibility for any injury to people or property resulting from any ideas, methods, instructions or products referred to in the content.